Published for SISSA by Springer

Received: November 8, 2011
Accepted: January 5, 2012
Published: January 25, 2012

Measurement of charm production at central rapidity in proton-proton collisions at $\sqrt{s} = 7$ TeV

The ALICE collaboration[1]

Abstract: The p_t-differential inclusive production cross sections of the prompt charmed mesons D^0, D^+, and D^{*+} in the rapidity range $|y| < 0.5$ were measured in proton-proton collisions at $\sqrt{s} = 7$ TeV at the LHC using the ALICE detector. Reconstructing the decays $D^0 \to K^-\pi^+$, $D^+ \to K^-\pi^+\pi^+$, $D^{*+} \to D^0\pi^+$, and their charge conjugates, about 8,400 D^0, 2,900 D^+, and 2,600 D^{*+} mesons with $1 < p_t < 24$ GeV/c were counted, after selection cuts, in a data sample of 3.14×10^8 events collected with a minimum-bias trigger (integrated luminosity $L_{int} = 5$ nb^{-1}). The results are described within uncertainties by predictions based on perturbative QCD.

Keywords: Hadron-Hadron Scattering

ArXiv ePrint: 1111.1553

[1]Corresponding author Andrea Dainese (andrea.dainese@pd.infn.it) on behalf of the ALICE Collaboration. Complete list of collaboration members at the end of the paper.

doi:10.1007/JHEP01(2012)128

Contents

1 Introduction

The study of the production of hadrons containing heavy quarks, i.e. charm and beauty, in proton-proton (pp) collisions at LHC energies provides a way to test, in a new energy domain, calculations of quantum chromodynamics (QCD) processes based on the factorization approach. In this scheme, cross sections are computed as a convolution of three terms: the parton distribution functions of the incoming protons, the partonic hard scattering cross section calculated as a perturbative series in the strong interaction coupling constant, and the fragmentation function, parametrizing the relative production yield and momentum distribution for a charm quark hadronizing to a particular species of D meson. Recent implementations of such calculations, at the perturbation level of next-to-leading order or at fixed order with next-to-leading-log resummation (FONLL) [1, 2] describe well the beauty production cross section measured in $\mathrm{p\overline{p}}$ collisions at $\sqrt{s} = 1.96$ TeV at the FNAL Tevatron collider [3–5] and in pp collisions at $\sqrt{s} = 7$ TeV at the CERN Large Hadron Collider (LHC) [6, 7]. The production cross section of charmed hadrons (D mesons) at Tevatron is reproduced within the theoretical uncertainties of the calculations as well [8–10]. However, the comparison suggests that charm production is underestimated by the results obtained with the central values of the calculation parameters, as observed also in pp collisions at the BNL RHIC collider at the lower energy of $\sqrt{s} = 200$ GeV [11–13]. In this context, it is particularly interesting to perform the comparison for charm production at the LHC energy, which is more than three times higher than at the Tevatron. Furthermore, at LHC energies, the measurement of charm production in the low transverse

JHEP01(2012)128

momentum ($p_{\rm t}$) region probes the parton distribution functions of the proton at small values of parton fractional momentum x and squared momentum transfer Q^2. For illustration, using a simplified $2 \to 2$ kinematics at leading order, c quarks ($m_{\rm c} \approx 1.5$ GeV/c^2) with $p_{\rm t} \sim 2$ GeV/c and rapidity $y \sim 0$ probe the parton distribution functions at $x \sim 7 \times 10^{-4}$ and $Q^2 \sim (5\ \text{GeV})^2$, where the gluon component is dominant. In this kinematic regime, the gluon distribution may reach the level of saturation, leading to a measurable departure of the observed cross sections from the expectations based on the factorization approach (see e.g. [14]).

We report on the measurement of the production cross section of the prompt charmed mesons $\rm D^0$, $\rm D^+$, and $\rm D^{*+}$, in pp collisions at $\sqrt{s} = 7$ TeV, reconstructed in the range $1 < p_{\rm t} < 24$ (16 for $\rm D^0$) GeV/c and $|y| < 0.5$ with the ALICE experimental apparatus [15], using data collected in 2010. The detector layout and the data sample used for the measurement are described in section 2. The D meson reconstruction procedure, the raw yield extraction, and the corrections applied to obtain the production cross sections, including the estimation of the prompt D meson fraction, are presented in sections 3 and 4. Finally, the resulting $p_{\rm t}$-differential cross sections are reported in section 4.3 and compared to QCD predictions.

2 Detector layout and data collection

$\rm D^0$, $\rm D^+$, and $\rm D^{*+}$ mesons, and their charge conjugates, are reconstructed from their decays into charged hadrons in the central rapidity region utilizing the tracking and particle identification capabilities of the ALICE central barrel detectors.

The ALICE apparatus is described in detail in [15]. It consists of a central barrel covering the pseudorapidity interval $|\eta| < 0.9$, a forward muon spectrometer, and a set of small detectors in the forward regions for trigger and event characterization purposes. Only the detector features that are relevant for the D meson analysis are presented here. The ALICE global coordinate system is right-handed, with the origin coinciding with the geometrical centre of the central barrel, the z axis directed along the beam line, the x axis in the LHC (horizontal) plane, pointing towards the centre of the accelerator, and the y axis pointing upward. The central barrel detectors are positioned within a large solenoid magnet, with a field B = 0.5 T, parallel to the beam line. Data collected with both magnet polarities were used for this analysis.

The innermost detector of the ALICE central barrel is the Inner Tracking System (ITS) which is made of six cylindrical layers of silicon detectors, with radial distance to the beam-line between 3.9 cm and 43.0 cm. The two innermost layers, with average radii of 3.9 cm (about 1 cm from the beam vacuum tube) and 7.6 cm, are equipped with Silicon Pixel Detectors (SPD), comprising $9.8{\times}10^6$ pixels of size $50\,(r\phi) \times 425\,(z)$ μm^2, with intrinsic spatial resolution of $12\,(r\phi) \times 100\,(z)$ μm^2. The signals of the 1,200 SPD readout chips provide a fast trigger through a programmable logic. The two intermediate layers, at radii of 15.0 and 23.9 cm, are made of Silicon Drift Detectors (SDD). They allow one to measure the hit position along z with resolution better than 30 μm from the centroid of signals collected on the anodes, and to determine the $r\phi$ coordinate from the drift time with a resolution that depends on the level of calibration, as discussed below. The two

JHEP01(2012)128

outermost layers are made of Silicon Strip Detectors (SSD), located at radii of 38.0 and 43.0 cm, consisting of double-sided silicon strip sensor modules, with an intrinsic spatial resolution of $20\,(r\phi) \times 830\,(z)$ μm^2. The total material budget of the ITS is on average 7.7% of radiation length for tracks crossing the ITS perpendicularly to the detector surfaces ($\eta = 0$) [15, 16]. These features enable measurement of the track impact parameter (i.e. the distance of closest approach of the track to the primary interaction vertex) in the bending plane ($r\phi$) with a resolution better than 75 μm for transverse momenta $p_{\rm t} > 1\,{\rm GeV}/c$ (see section 3.1).

The ITS modules were aligned using survey information, cosmic-ray tracks, and pp data, with the methods described in [16]. For the residual misalignment along the $r\phi$ coordinate, a r.m.s. of about 8 μm for SPD and 15 μm for SSD modules was estimated [16, 17]. For SDD, with the current calibration level, the space point resolution along $r\phi$ is ≈ 60 μm for those modules (about 60% of the total) that do not suffer from significant drift field non-uniformities. To account for the fact that a correction for these effects was not applied in the reconstruction of 2010 data, a systematic uncertainty of 300 μm was assumed for SDD points. Along z, the estimated precision of the alignment is 50 μm for SPD and SDD and a few hundred μm for SSD. These values are added in quadrature to the uncertainty on the reconstructed ITS hits in the track reconstruction algorithm. In the detector simulation, to account in an effective way for the residual misalignment, the ITS modules are randomly displaced with respect to their ideal positions according to the estimated precision of the alignment.

At larger radii ($85 < r < 247$ cm), the cylindrical Time Projection Chamber (TPC) [18] provides track reconstruction with up to 159 three-dimensional space points per track, as well as particle identification via the measurement of the specific energy deposit ${\rm d}E/{\rm d}x$. The TPC has an active length of 500 cm along the z direction and its 90 m^3 gas volume is filled with a mixture composed of Ne (85.7%), CO_2 (9.5%), and N_2 (4.8%). Its position resolution is 1100–1250 μm along the z axis (corresponding to the drift direction) and 800–1100 μm along $r\phi$. Using cosmic-ray muons and data taken in pp collisions, the relative ${\rm d}E/{\rm d}x$ resolution was measured to be about 5.5% for tracks that cross the entire detector [18].

The charged particle identification capability of the TPC is supplemented by the Time-Of-Flight detector (TOF), that is based on Multi-gap Resistive Plate Chambers (MRPCs) in a cylindrical configuration at radius 370–399 cm from the beam axis, with readout consisting of 152,928 sensitive pads of dimension 2.5×3.5 cm^2. The TOF resolution on the particle arrival time is at present better than 100 ps. The start time of the collision (event time zero) is measured by the T0 detector, an array of Cherenkov counters located at +350 cm and −70 cm along the beam-line, or, for the events in which the T0 signal is not present, estimated using the particle arrival times at the TOF. The particle identification is based on the difference between the measured time-of-flight and its expected value, computed for each mass hypothesis from the track momentum and length. The overall resolution on this difference is about 160 ps. In this analysis, the time-of-flight measurement provides kaon/pion separation up to a momentum of about 1.5 GeV/c. Results from the TOF commissioning with cosmic-ray particles are reported in [19].

JHEP01(2012)128

The data sample used for the analysis presented here consists of 314 million minimum-bias (MB) events, corresponding to an integrated luminosity $L_{\rm int} = 5$ nb^{-1}, collected during the 2010 LHC run with pp collisions at $\sqrt{s} = 7$ TeV. The minimum-bias trigger was based on the SPD and VZERO detectors. The VZERO detector consists of two arrays of 32 scintillators each, placed around the beam vacuum tube on either side of the interaction region. The two arrays cover the pseudorapidity ranges $-3.7 < \eta < -1.7$ and $2.8 < \eta < 5.1$. Minimum-bias collisions were triggered by requiring at least one hit in either of the VZERO counters or in the SPD ($|\eta| < 2$), in coincidence with the arrival of proton bunches from both directions. This trigger was estimated to be sensitive to about 87% of the pp inelastic cross section [20, 21]. It was verified on Monte Carlo simulations based on the PYTHIA 6.4.21 event generator [22] (with Perugia-0 tuning [23]) that the minimum-bias trigger is 100% efficient for D mesons with $p_{\rm t} > 1$ GeV/c and $|y| < 0.5$. Contamination from beam-induced background was rejected offline using the timing information from the VZERO and the correlation between the number of hits and track segments (tracklets) in the SPD detector. The instantaneous luminosity in the ALICE experiment was limited to 0.6–1.2×10^{29} cm^{-2}s^{-1} by displacing the beams in the transverse plane by 3.8 times the r.m.s of their transverse profile. In this way, the interaction probability per bunch crossing was kept in the range 0.04–0.08, with probability of collision pile-up below 4% per triggered event. The luminous region was measured with high precision from the distribution of the interaction vertices reconstructed from the charged particles tracked in the ALICE central barrel detectors, yielding $\sigma_x^{\rm luminous} \approx \sigma_y^{\rm luminous} \approx 35$–$50$ μm in the transverse plane and $\sigma_z^{\rm luminous} \approx 4$–$6$ cm along the beam direction (the quoted ranges are due to the variations of the beam conditions during the data taking). Only events with interaction vertex in the range $|z| < 10$ cm were used for the analysis.

3 Reconstruction of D meson decays

The measurement of charm production was performed by reconstructing three decay modes for D mesons, $\rm D^0 \to K^-\pi^+$ (with branching ratio, BR, of $3.87 \pm 0.05\%$), $\rm D^+ \to K^-\pi^+\pi^+$ (BR of $9.13 \pm 0.19\%$), and $\rm D^*(2010)^+ \to D^0\pi^+$ (strong decay with BR of $67.7 \pm 0.5\%$) with $\rm D^0 \to K^-\pi^+$, together with their charge conjugates [24]. The $\rm D^0$ and $\rm D^+$ mesons have mean proper decay lengths $c\tau \approx 123$ and 312 μm, respectively [24]. Their decay secondary vertices are therefore typically displaced by a few hundred μm from the primary vertex of the pp interaction. The analysis strategy for the extraction of the $\rm D^0$ and $\rm D^+$ signals from the large combinatorial background due to uncorrelated tracks is based on the reconstruction and selection of secondary vertex topologies that have significant separation from the primary vertex. The identification of the charged kaons in the TPC and TOF detectors provides additional background rejection in the low-momentum region. A particle identification strategy that has high efficiency for the D meson signal (see section 4.1) was adopted. Finally, an invariant mass analysis was used to extract the signal yield. In the $\rm D^{*+} \to D^0\pi^+$ case, the decay vertex cannot be resolved from the primary vertex. The analysis exploits topological selections on the $\rm D^0$, together with the sharp peak in the difference between the invariant mass of the three final state hadrons and that of the two

JHEP01(2012)128

D^0 decay prongs. Given that the mass difference $\Delta m = m_{\mathrm{D}^{*+}} - m_{\mathrm{D}^0} \approx 145.4$ MeV/c^2 [24] is only slightly larger than the charged pion mass, for low p_{t} D^{*+} mesons the produced pion has low momentum and is referred to here as a 'soft pion'.

3.1 Track and vertex reconstruction

The procedure for track reconstruction in the central barrel detectors [15, 25] starts with a first determination of the primary vertex position, performed by correlating hit pairs (tracklets) in the two layers of the Silicon Pixel Detector. The same algorithm is used to search for vertices from pile-up collisions starting from the tracklets that do not point to the first found vertex. An event is rejected from the analyzed data sample if a second interaction vertex is found, it has at least 3 associated tracklets, and it is separated from the first one by more than 8 mm. The remaining undetected pile-up is negligible for the analysis described in this paper. Track seeds are built using this first estimate of the interaction vertex position together with pairs of reconstructed space points in adjacent readout pad rows of the TPC. Tracks are then projected inward in the radial direction using a Kalman filter algorithm, incorporating space points in the TPC and then hits in the six layers of the ITS (referred to here as TPC+ITS tracks). The ITS hits not associated to TPC+ITS tracks by this procedure are then used to search for ITS-only tracks, most importantly to recover pions with $80 < p_{\mathrm{t}} < 200$ MeV/c that have very low reconstruction efficiency in the TPC, for geometrical reasons. ITS-only tracks are found using a hit grouping algorithm that projects angular windows radially outward from the primary vertex. The TPC+ITS tracks are then propagated outward in order to associate signals in the large-radius detectors that perform particle identification. Finally, all tracks are re-propagated with the Kalman filter in the inward direction. The relative p_{t} resolution at the primary vertex for this procedure is about 1% (6%) at 1 GeV/c for TPC+ITS (ITS-only) tracks. The last step of event reconstruction is the re-determination of the primary vertex position from the accepted tracks [26]. The primary vertex coordinates and covariance matrix are obtained via an analytic χ^2 minimization method applied to the tracks approximated by straight lines after propagation to their common point of closest approach. The algorithm is then repeated excluding the tracks with distance to the primary vertex, normalized to its estimated uncertainty, larger than 3, which are incompatible with being produced by primary particles. The vertex fit is constrained in the transverse plane using the information on the position and spread $\sigma_{x,y}^{\mathrm{luminous}}$ of the luminous region. The latter is determined from the distribution of primary vertices averaged over the run and is tabulated as a function of time during the full data-taking period. The position resolution of the primary vertex reconstructed from tracks depends on the particle multiplicity. It was measured to be $\sigma_z\,(\mu\mathrm{m}) \approx 430/N_{\mathrm{tracklets}}^{0.7}$ in the longitudinal direction and $\sigma_{x,y}\,(\mu\mathrm{m}) \approx \min(\sigma_{x,y}^{\mathrm{luminous}}, 600/N_{\mathrm{tracklets}}^{0.9})$ in the transverse coordinates by fitting its dependence on the number of tracklets in the SPD ($N_{\mathrm{tracklets}}$), which corresponds to about twice the multiplicity of primary charged particles per unit of rapidity. Thus, for the average luminous region spread $\sigma_{x,y}^{\mathrm{luminous}} \approx 40$ μm, the transverse position of the vertex has a resolution that ranges from 40 μm in low-multiplicity events (i.e. below 10 charged particles per unit of rapidity) to about 10 μm in events with a multiplicity of about 40.

JHEP01(2012)128

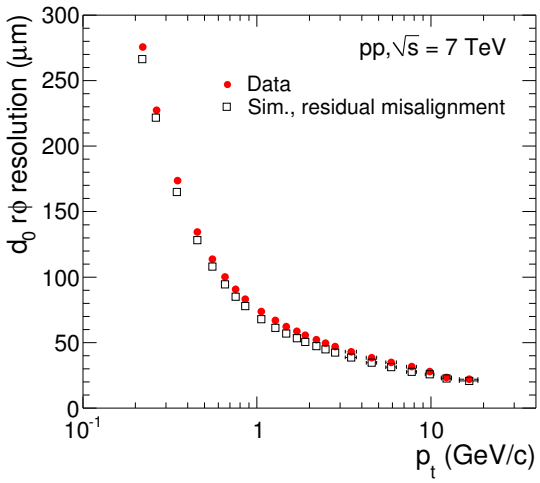

Figure 1. Track impact parameter (d_0) resolution in the transverse plane ($r\phi$ direction) as a function of $p_{\rm t}$ comparing data and simulation. This resolution includes the uncertainty in the primary vertex position, which is reconstructed excluding the track being probed.

Secondary vertices of $\rm D^0$ and $\rm D^+$ meson candidates were reconstructed using tracks having $|\eta| < 0.8$, $p_{\rm t} > 0.4$ GeV/c, at least 70 associated space points (out of a maximum of 159) and $\chi^2/\mathrm{ndf} < 2$ in the TPC, and at least one hit in either of the two layers of the SPD. For tracks passing this selection, the average number of hits in the six ITS layers is 4.5–4.7, depending on the data taking period. This quantity is influenced by the fraction of inactive channels and its distribution is well reproduced in Monte Carlo simulations. For the $\rm D^{*+}$ soft pion, all TPC+ITS and ITS-only tracks with at least 4 hits in the ITS, including at least one in the SPD, and $p_{\rm t} > 80$ MeV/c were considered. Figure 1 shows the transverse momentum dependence of the transverse ($r\phi$) impact parameter (d_0) resolution achieved with the present ITS alignment precision for tracks that satisfy the TPC and ITS selection criteria, for data and Monte Carlo simulations. The simulations utilize GEANT3 [27] and incorporate a detailed description of the detector material, geometry and response. Proton-proton collisions were simulated using the PYTHIA 6.4.21 event generator [22] with Perugia-0 tuning [23]. The impact parameter resolution was estimated by fitting the inclusive distribution of d_0 with respect to the event primary vertex, in intervals of $p_{\rm t}$. The fit function is the sum of a Gaussian, that accounts for the component due to prompt particles produced at the primary vertex, and two exponential functions, that account for secondary particles, mainly from weak decays of strange hadrons. The width σ of the Gaussian provides an estimate of the d_0 resolution, which includes the resolution of the track parameters and the primary vertex position. In order to obtain an unbiased estimate of d_0, the primary vertex is recalculated excluding the track being probed. The figure shows that the d_0 resolution measured in data, with values of 75 (20) μm at $p_{\rm t} = 1$ (15) GeV/c, is reproduced within about 10% by the Monte Carlo simulation incorporating the residual ITS misalignment described in section 2. The effect of the difference between data and simulation on the results of the D meson analysis is discussed in section 4.2.

JHEP01(2012)128

3.2 D meson selection

D^0, D^+, and D^{*+} candidates were filtered by applying kinematical and topological cuts, and particle identification criteria. A fiducial acceptance cut $|y_D| < y_{fid}(p_t)$ was applied, with y_{fid} smoothly increasing from 0.5 to 0.8 in $0 < p_t < 5$ GeV/c and $y_{fid} = 0.8$ above 5 GeV/c. For D^0 and D^+ decays, the secondary vertex was reconstructed with the same algorithm used to compute the primary vertex from tracks. The resolution on the position of D^0 and D^+ decay vertices was estimated by Monte Carlo simulations to be of the order of 100 μm with little p_t-dependence for $p_t > 1$ GeV/c [26]. For the D^0 and D^+ selection, the primary vertex was recalculated for each D candidate, excluding the decay tracks.

The cut variables for the three mesons are described in the following. The actual cut values are p_t dependent and were tuned to optimize the statistical significance of the signal, resulting in a selection efficiency that increases with increasing p_t. The cut values applied for D mesons at low p_t are reported for reference in the next paragraphs.

For D^0 mesons, the two decay candidate tracks were further selected with $p_t > 0.7$ GeV/c ($p_t > 0.4$ GeV/c for $1 < p_t^{D^0} < 2$ GeV/c) and $r\phi$ impact parameter significance $|d_0|/\sigma_{d_0} > 0.5$. Secondary vertices were required to have a minimum displacement of 100 μm from the primary vertex and a maximum distance of closest approach between the two tracks of 300 μm. The cut $|\cos\theta^*| < 0.8$, where θ^* is the angle between the kaon momentum in the D^0 rest frame and the boost direction, was applied to reduce the contamination of background candidates that do not represent real two-body decays and typically have large values of $|\cos\theta^*|$. Well-displaced $D^0 \to K^-\pi^+$ topologies are characterized by large and opposite-sign values of the decay track $r\phi$ impact parameters (d_0^π and d_0^K) and good pointing of the reconstructed D^0 momentum to the primary vertex, i.e. a small value of the pointing angle $\theta_{pointing}$ between the momentum and flight line. Due to the strong correlation of these two features in the signal, the requirement $d_0^\pi \times d_0^K < -(120\ \mu m)^2$ and $\cos\theta_{pointing} > 0.8$ was found to be effective in increasing the signal-to-background ratio.

The D^+ selection is based on a similar strategy to that for D^0 mesons. A looser cut on the p_t of decay tracks, 0.4 GeV/c, was applied, due to the lower average momentum of the products of a three-body decay. The candidate triplets were selected on the basis of the sum of the distances of the decay tracks to the reconstructed decay vertex, the decay length, the cosine of the pointing angle, and the sum of the squares of the $r\phi$ impact parameters of the three tracks. Typical cut values for low-p_t candidates are: decay length larger than 800 μm, $\cos\theta_{pointing} > 0.95$, and sum of the squares of the three decay tracks impact parameters $\Sigma\, d_0^2 > (750\ \mu m)^2$. The topological selection cuts are, in general, tighter than for the D^0 case due to the larger $c\tau$ of the D^+ meson, resulting in a better separation between primary and secondary vertices, and to the higher combinatorial background in the three-particle final state.

The D^{*+} candidates were filtered by applying kinematical selections on the final decay products and cuts on the topology of the D^0 decay. The single track minimum transverse momentum was set to 0.4 GeV/c for the D^0 decay tracks and 80 MeV/c for the soft pion track. The variables used to select the topology of the D^0 decay are the same as for the D^0 analysis described above. However, a selection with higher efficiency could be applied in

JHEP01(2012)128

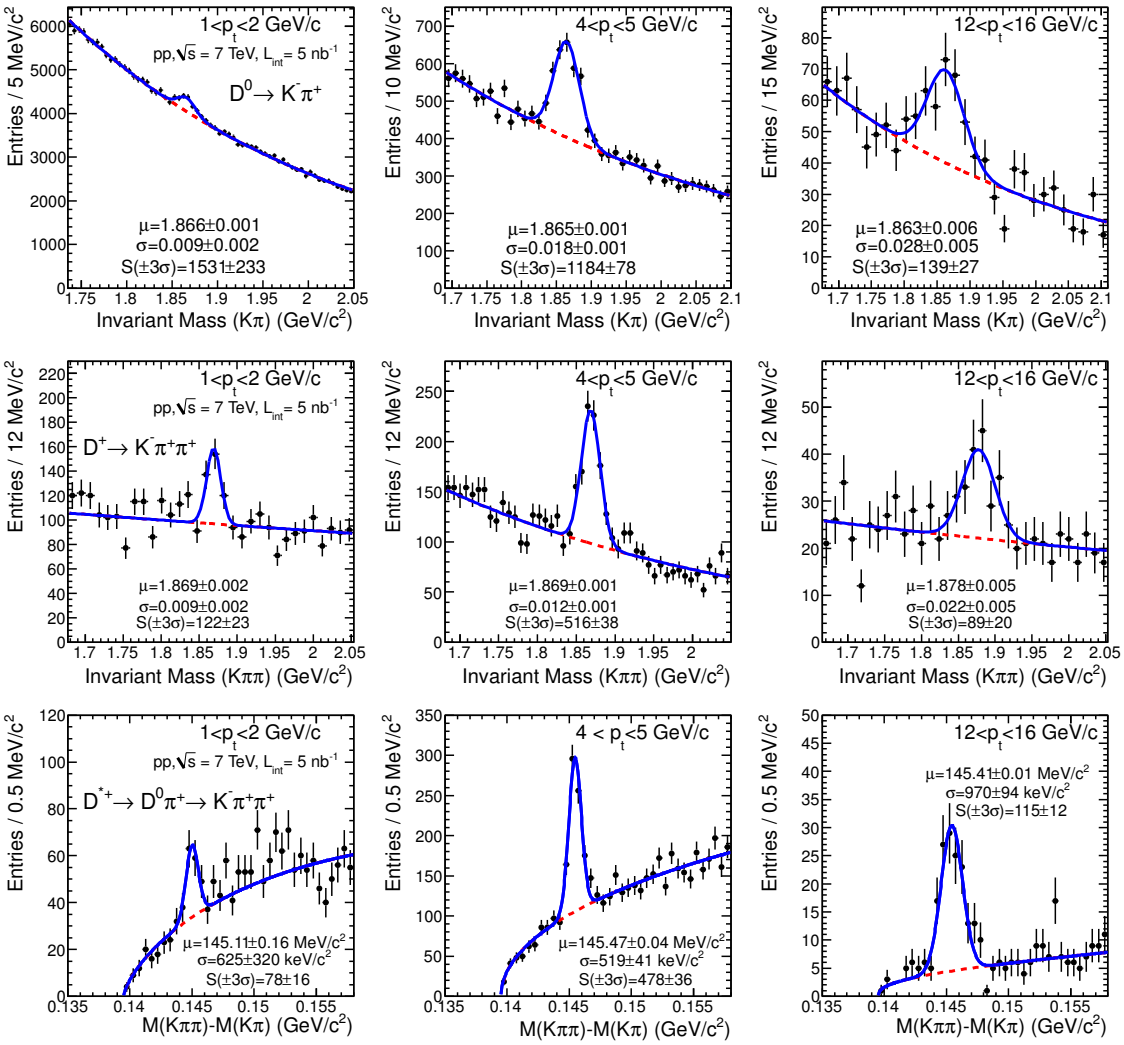

Figure 2. Invariant mass distributions for D^0 (top) and D^+ (middle) candidates, and mass difference distribution for D^{*+} candidates (bottom), for three p_{t} intervals. The curves show the fit functions as described in the text. The values of mean (μ) and width (σ) of the signal peak are reported (for D^0 and D^+ they are expressed in GeV/c^2).

this case, because the background in the region around $\Delta m \approx 145$ MeV/c^2, which is close to the phase space boundary, is much lower than that around the D^0 mass. In particular, for D^{*+} candidates with $p_{\mathrm{t}} > 6$ GeV/c, the topological cuts could be opened so as to select about 90% of the signal passing single track cuts.

The particle identification selection used the specific energy deposit and the time-of-flight from the TPC and TOF detectors, respectively. In order to assign the kaon or pion mass to the decay tracks, compatibility cuts were applied to the difference between the measured and expected signals. For both $\mathrm{d}E/\mathrm{d}x$ and time-of-flight, a $3\,\sigma$ compatibility cut was used. Tracks without a TOF signal were identified using only the TPC information,

JHEP01(2012)128

p_{t} interval	$N \pm$ stat. $\pm$ syst.		
(GeV/c)	$\mathrm{D}^0 + \overline{\mathrm{D}}^0$	$\mathrm{D}^+ + \mathrm{D}^-$	$\mathrm{D}^{*+} + \mathrm{D}^{*-}$
1–2	$1531 \pm 233 \pm 340$	$122 \pm 23 \pm 30$	$78 \pm 16 \pm 8$
2–3	$1978 \pm 168 \pm 190$	$390 \pm 57 \pm 97$	$244 \pm 26 \pm 10$
3–4	$1950 \pm 129 \pm 75$	$405 \pm 40 \pm 101$	$363 \pm 29 \pm 11$
4–5	$1184 \pm 78 \pm 40$	$516 \pm 38 \pm 46$	$478 \pm 36 \pm 14$
5–6	$623 \pm 50 \pm 25$	$361 \pm 31 \pm 33$	$374 \pm 28 \pm 18$
6–7	$339 \pm 32 \pm 13$	$294 \pm 30 \pm 15$	$279 \pm 22 \pm 14$
7–8	$199 \pm 25 \pm 14$	$213 \pm 27 \pm 11$	$170 \pm 19 \pm 9$
8–12	$427 \pm 38 \pm 30$	$434 \pm 30 \pm 22$	$408 \pm 28 \pm 18$
12–16	$139 \pm 27 \pm 14$	$89 \pm 20 \pm 9$	$115 \pm 12 \pm 10$
16–24	—	$52 \pm 14 \pm 5$	$41 \pm 6 \pm 8$

Table 1. Measured raw yields for D^0, D^+, and D^{*+} mesons, and their anti-particles, in a minimum-bias pp sample corresponding to 5 nb^{-1} at $\sqrt{s} = 7$ TeV, in transverse momentum intervals. The systematic uncertainty estimation is described in section 4.2.

and tracks with incompatible TOF and TPC indications were treated as non-identified, but still used in the analysis and considered to be compatible with both a pion and a kaon. Two-prong candidates were accepted (as D^0, $\overline{\mathrm{D}}^0$, or both) or rejected, according to the compatibility with the $\mathrm{K}^{\mp}\pi^{\pm}$ final state. For D^0 candidates used in D^{*+} reconstruction, compatibility with the appropriate final state, consistent with the soft pion charge, was required. Particle identification was not applied to the soft pion tracks. In the case of the $\mathrm{D}^+ \to \mathrm{K}^-\pi^+\pi^+$ decay, the particle with the opposite charge sign with respect to the D meson is a kaon. Hence, the triplets were rejected if the opposite sign track was not compatible with the kaon hypothesis, or at least one of the two same sign tracks was not compatible with the pion hypothesis. For all three D meson species, a comparison of the invariant mass distributions obtained without and with particle identification shows that this selection reduces the combinatorial background by a factor 2–3 in the low p_{t} region, while preserving close to 100% of the D meson signal.

The raw signal yields were extracted in the intervals of p_{t} listed in table 1, by a fit to the invariant mass distributions (or mass difference for the D^{*+}), as shown in figure 2 for three selected p_{t} intervals. For D^0 and D^+ mesons, the fitting function consists of a Gaussian describing the signal and an exponential term for the background. In the D^0 case, the contribution of signal candidates with wrong mass assignment to the final state hadrons is also present in the invariant mass spectrum. It was verified on Monte Carlo simulations that this does not bias the extracted signal yield, because the invariant mass distribution of these candidates is wide enough to be accounted for by the background function. Moreover, at low p_{t}, the particle identification selection strongly suppresses this

JHEP01(2012)128

contribution. For D^{*+} mesons, the mass difference Δm distribution is fitted using a function that consists of a Gaussian describing the signal and the term $a\sqrt{\Delta m - m_\pi}\cdot \mathrm{e}^{b(\Delta m - m_\pi)}$ for the background [8], where m_π is the charged pion mass, and a and b are free parameters. For all three D meson species, the mean of the Gaussian is compatible with the PDG value [24] within errors, and its width is well reproduced in the simulation. The extracted D meson raw yields are reported in table 1.

4 D meson cross sections

4.1 Corrections

The production cross sections of prompt charmed mesons were calculated as (e.g. for D^+):

$$\left.\frac{\mathrm{d}\sigma^{\mathrm{D}^+}}{\mathrm{d}p_\mathrm{t}}\right|_{|y|<0.5} = \frac{1}{2}\frac{1}{\Delta y\,\Delta p_\mathrm{t}}\frac{f_\mathrm{prompt}(p_\mathrm{t})\cdot N^{\mathrm{D}^\pm\ \mathrm{raw}}(p_\mathrm{t})\Big|_{|y|<y_\mathrm{fid}}}{(\mathrm{Acc}\times\epsilon)_\mathrm{prompt}(p_\mathrm{t})\cdot \mathrm{BR}\cdot L_\mathrm{int}}\,. \tag{4.1}$$

$N^{\mathrm{D}^\pm\ \mathrm{raw}}(p_\mathrm{t})$ is the measured inclusive raw yield, obtained from the invariant mass analysis in each p_t interval (of width Δp_t); f_prompt is the prompt fraction of the raw yield; $(\mathrm{Acc}\times\epsilon)_\mathrm{prompt}$ is the acceptance times efficiency of prompt mesons, where ϵ accounts for vertex reconstruction, track reconstruction and selection, and for D meson candidate selection with the secondary vertex and particle identification cuts described in section 3. Δy $(= 2\,y_\mathrm{fid})$ is the width of the fiducial rapidity coverage (see section 3.2) and BR is the decay branching ratio [24]. The factor 1/2 accounts for the fact that the measured yields include particles and anti-particles while the cross sections are given for particles only. The integrated luminosity was computed as $L_\mathrm{int} = N_\mathrm{pp,MB}/\sigma_\mathrm{pp,MB}$, where $N_\mathrm{pp,MB}$ and $\sigma_\mathrm{pp,MB}$ are the number and the cross section, respectively, of pp collisions passing the minimum-bias trigger condition defined in section 2. The $\sigma_\mathrm{pp,MB}$ value, 62.5 mb, was derived from a measurement using a van der Meer scan [28] of the cross section of collisions that give signals in both sides of the VZERO scintillator detector ($\sigma_\mathrm{VZERO\text{-}AND}$) [20, 21]. The normalization factor, $\sigma_\mathrm{pp,VZERO\text{-}AND}/\sigma_\mathrm{pp,MB} \approx 0.87$, was found to be stable within 1% in the data sample. The uncertainty on $\sigma_\mathrm{pp,MB}$ is determined by the systematic uncertainty of 3.5% on $\sigma_\mathrm{VZERO\text{-}AND}$, which is due to the uncertainties on the beam intensities [29] and on the analysis procedure related to the van der Meer scan of the signal.

The rapidity acceptance correction, using the factor $2\,y_\mathrm{fid}$, with y_fid varying from 0.5 at low p_t to 0.8 at high p_t, assumes that the rapidity distribution of D mesons is uniform in the range $|y| < y_\mathrm{fid}$. This assumption was checked using the PYTHIA 6.4.21 event generator [22] with Perugia-0 tuning [23] and the FONLL pQCD calculation [1, 2, 30], both of which generate a D meson yield that is uniform within 1% in the range $|y| < 0.8$. The $(\mathrm{Acc}\times\epsilon)$ correction was determined using Monte Carlo simulations based on the GEANT3 transport code [27]. The luminous region distribution and the conditions of all the ALICE detectors in terms of active channels, gain, noise level, and alignment, and their evolution with time during the 2010 LHC run, were included in the simulations. Proton-proton collisions were simulated using the PYTHIA 6.4.21 event generator [22] with Perugia-0

JHEP01(2012)128

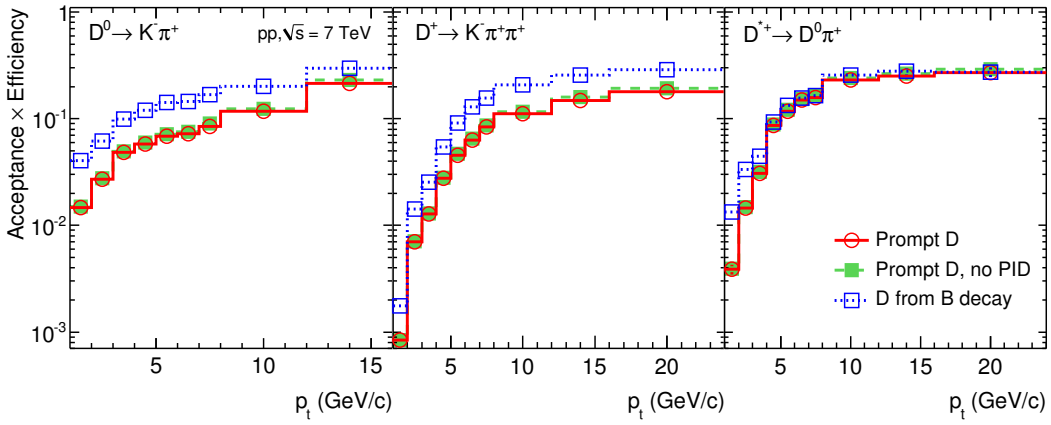

Figure 3. Acceptance × efficiency for D^0, D^+, and D^{*+} mesons, as a function of p_t (see text for details).

tuning [23]. Only events containing D mesons were transported through the apparatus and reconstructed, and the efficiency was extracted separately for prompt D mesons and D mesons from B meson decays. Figure 3 shows, as a function of transverse momentum, the acceptance times efficiency (Acc × ϵ) for D^0, D^+, and D^{*+} mesons with $|y| < y_{\rm fid}$. At low p_t, the efficiencies are of order 1% or less, while for large p_t the efficiencies increase and flatten at about 10-20% for D^0 and D^+, and 30% for D^{*+}. The efficiencies without particle identification selection, shown for comparison, are the same as those with particle identification, indicating that this selection is essentially fully efficient for the signal. The efficiencies for D^0 and D^+ mesons from B meson decays, also shown for comparison, are larger by about a factor of two. This behaviour is due to the fact that feed-down D mesons decay further from the primary vertex, because of the large B meson lifetime ($c\tau \approx 500\ \mu$m [24]). For D^{*+} mesons, the efficiency for the prompt and feed-down components are the same in the p_t range above 4 GeV/c, where no strong cuts on the separation of the D^0 decay vertex from the primary vertex are applied.

The fraction $f_{\rm prompt}$ of D mesons coming from c quark hadronization, i.e. the correction factor that accounts for the feed-down from B meson decays, was evaluated using the B production cross section from the FONLL pQCD calculation [1, 2, 30], which describes well beauty production at Tevatron [4] and at the LHC [6, 7], and the B → D decay kinematics from the EvtGen package [31]. The computed cross section for the feed-down component for each of the three D meson species was used, together with the Monte Carlo acceptance times efficiency $(\mathrm{Acc}\times\epsilon)_{\rm feed\text{-}down}$ for D mesons from B decays (see figure 3), to compute the expected feed-down contribution in the measured raw yields:

$$f_{\rm prompt} = 1 - (N^{\rm D^\pm\ from\ B\ raw}/N^{\rm D^\pm\ raw}) \tag{4.2}$$

with:

$$N^{\rm D^\pm\ from\ B\ raw}\Big|_{|y|<y_{\rm fid}} = 2\,\frac{{\rm d}\sigma^{\rm D^+\ from\ B}_{\rm FONLL}}{{\rm d}p_t}\Bigg|_{|y|<0.5} \cdot \Delta y\,\Delta p_t \cdot (\mathrm{Acc}\times\epsilon)_{\rm feed\text{-}down} \cdot \mathrm{BR} \cdot L_{\rm int}\,. \tag{4.3}$$

JHEP01(2012)128

The symbol of the $p_{\rm t}$-dependence ($p_{\rm t}$) is omitted in the formulas, for brevity. The resulting prompt fraction $f_{\rm prompt}$ is shown in figure 4 (left-hand panel) by the solid horizontal lines, for the case of $\rm D^0$ mesons. The prompt fraction ranges between 80% and 90%, depending on the $p_{\rm t}$ interval, these values being determined also by the different efficiencies for prompt and feed-down D mesons. In order to estimate the systematic uncertainty, the perturbative uncertainty on the FONLL beauty production cross section was considered, as well as an alternative way of using the FONLL calculation. The former contribution was obtained by varying the b quark mass and the factorization and renormalization scales as suggested in, e.g., [32]. The alternative method consisted of computing the prompt fraction using the FONLL cross sections for prompt and feed-down D mesons (with $\rm B \to D$ via EvtGen [31] for the latter) and their respective Monte Carlo efficiencies:

$$f_{\rm prompt} = \left(1 + \frac{(\mathrm{Acc} \times \epsilon)_{\text{feed-down}}}{(\mathrm{Acc} \times \epsilon)_{\rm prompt}} \frac{\left.\frac{\mathrm{d}\sigma^{\rm D^+\ from\ B}_{\rm FONLL}}{\mathrm{d}p_{\rm t}}\right|_{|y|<0.5}}{\left.\frac{\mathrm{d}\sigma^{\rm D^+}_{\rm FONLL}}{\mathrm{d}p_{\rm t}}\right|_{|y|<0.5}} \right)^{-1} . \tag{4.4}$$

The resulting prompt fraction is shown by the dashed horizontal lines in figure 4 (left-hand panel). The full envelope of the uncertainty bands from the two methods, which is shown by the boxes in the figure, was taken as a systematic uncertainty. The uncertainty related to the B decay kinematics was disregarded, after verifying that the difference resulting from using the PYTHIA [22] decayer instead of EvtGen [31] is negligible with respect to the FONLL B meson cross section uncertainty.

The prompt fraction of $\rm D^0$ mesons in the reconstructed yield was also estimated with a data-driven method based on the measured impact parameter distribution of $\rm D^0$ meson candidates in each $p_{\rm t}$ interval, as done previously by the CDF Collaboration [8]. This method exploits the different shapes of the distributions of the impact parameter to the primary vertex of prompt and feed-down (displaced) D mesons. The impact parameter distribution of $\rm D^0$ mesons was obtained from the one measured for candidates with invariant mass in the range $|m - M_{\rm D^0}| < 2\,\sigma$, after subtracting the background contribution estimated from the candidates in the side-bands (in the range $4.5\,\sigma < |m - M_{\rm D^0}| < 4.5\,\sigma + 100$ MeV/c^2). The prompt fraction was estimated by fitting the resulting impact parameter distribution with a two-component function. The first component is a detector resolution term, modelled by a Gaussian and an exponential term, describing the impact parameter of prompt D mesons. The second component accounts for the reconstructed impact parameter distribution of D from B decay, which is modelled by a convolution of the same detector resolution term with a double-exponential function describing the true impact parameter of secondary D mesons. The fit parameters are the width of the Gaussian and the fraction of prompt D mesons, that is, the relative weight of the prompt and secondary D meson components. An example of such a fit is shown in figure 4 (right-hand panel) for the $\rm D^0$ mesons in the transverse momentum interval $2 < p_{\rm t} < 3$ GeV/c. The prompt fraction of $\rm D^0$ mesons, measured with this method for $2 < p_{\rm t} < 12$ GeV/c, is shown by the circles in figure 4 (left-hand panel) and is found to be in general agreement with the FONLL-based estimations. Because of the large background for $p_{\rm t} < 2$ GeV/c and the poor statistics

JHEP01(2012)128

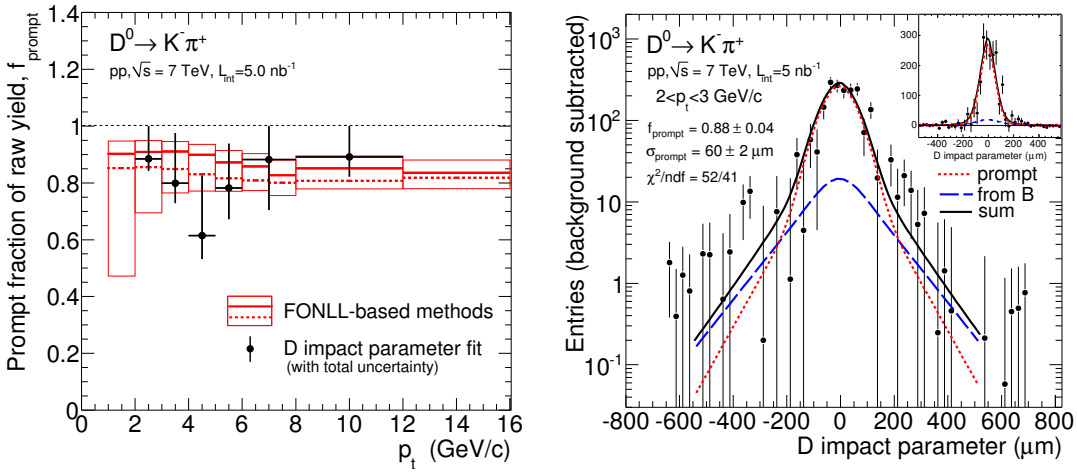

Figure 4. Left: prompt fraction $f_{\rm prompt}$ of the $\rm D^0$ raw yield as a function of $p_{\rm t}$, for the two FONLL-based methods (solid: central value, from eq. (4.2); dashed: alternative method, from eq. (4.4)) and for the impact parameter fit method (circles); the boxes show the envelope of the uncertainty bands of the two FONLL-based methods; the error bars show the total uncertainty from the impact parameter fit, including the statistical and systematic contributions. Right: an example of $\rm D^0$ meson impact parameter distribution in the transverse plane, for $2 < p_{\rm t} < 3$ GeV/c; the distribution is background-subtracted and fitted with the two-component function for prompt and feed-down contributions, as described in the text; the resulting prompt fraction, impact parameter resolution for prompt mesons, and χ^2/(number of degrees of freedom) of the fit are given; the inset, with linear scale, shows also the negative entries, resulting from the background subtraction.

available for $p_{\rm t} > 12$ GeV/c, this method was used only as a check of the FONLL-based prompt fraction estimation, for the $p_{\rm t}$ intervals with large signal yield.

4.2 Systematic uncertainties

Several sources of systematic uncertainty were considered, including those affecting the signal extraction from the invariant mass spectra and all the correction factors applied to obtain the $p_{\rm t}$-differential cross sections. A summary of the estimated relative systematic uncertainties is given in table 2, for the lowest and highest $p_{\rm t}$ interval (see table 1) for each meson species. All the uncertainties evolve monotonously as a function of $p_{\rm t}$, except for the yield extraction and feed-down correction contributions, which are larger at low and high $p_{\rm t}$ than at intermediate $p_{\rm t}$.

The systematic uncertainty on the yield extraction from the invariant mass spectrum in a given $p_{\rm t}$ interval was determined by repeating the fit in a different mass range, and also varying the function to describe the background. A polynomial, instead of an exponential, was used for $\rm D^0$ and $\rm D^+$ mesons, while a power law convoluted with an exponential and a polynomial was considered for $\rm D^{*+}$ mesons, instead of the function defined in section 3.2. A method based on bin counting (after subtraction of the background estimated from a fit in the mass side bands) was also used. The uncertainty was defined as the maximum variation in the extracted yields from these different methods.

JHEP01(2012)128

	D^0		D^+		D^{*+}	
	Low p_t	High p_t	Low p_t	High p_t	Low p_t	High p_t
Raw yield extraction	20%	10%	25%	10%	10%	20%
Tracking efficiency	8%		12%		13%	12%
Cut efficiency	10%	10%	10%	10%	22%	10%
PID efficiency	5%	3%	15%	5%	4%	3%
MC p_t shape	3%	1%	3%	1%	3%	1%
Feed-down from B	$^{+\ 5}_{-45}$%	$^{+\ 8}_{-10}$%	$^{+\ 3}_{-40}$%	$^{+\ 8}_{-10}$%	$^{+\ 4}_{-45}$%	$^{+3}_{-7}$%
Branching ratio	1.3%		2.1%		1.5%	
Normalization	3.5%					

Table 2. Summary of relative systematic uncertainties for the lowest and highest p_t interval for each meson species.

The systematic uncertainty related to the tracking efficiency includes the effects arising from track finding in the TPC, from track propagation from the TPC to the ITS, and from track quality selection. It was estimated from the comparison of data and simulation and from the variation of the track selection. The resulting uncertainty is 8% for the two-body decay of D^0 mesons and 12% for the three-body decay of D^+ mesons. For the D^{*+} case, a slightly larger systematic uncertainty of 13% was assigned in the low p_t region (below 3 GeV/c), because the soft pion often has $p_t < 150$ MeV/c and is reconstructed only in the ITS. The tracking efficiency in this case has a significant uncertainty arising from the description of hadronic interactions in the simulation of the detector response.

A systematic effect can arise due to residual discrepancies between data and simulation for the variables used to select the signal D meson candidates. The distributions of these variables were compared for candidates passing loose topological cuts, i.e. essentially for background candidates, and found to be well described in the simulation. The systematic effects due to residual differences between data and simulation were quantified by repeating the analysis with different sets of cuts. In particular, the cut values were changed in order to vary the signal by at least 20% below $p_t = 8$ GeV/c. From the corresponding variation of the corrected spectra, a systematic uncertainty of about 10% was estimated for each D meson species. As a further cross-check, the secondary vertices in the simulation were reconstructed also after a track-by-track scaling by a factor 1.08 of the impact parameter residuals with respect to their true value. This scaling is aimed at reproducing the impact parameter resolution observed in the data (see figure 1) and accounts for possible residual detector misalignment effects not fully described in the simulation. The resulting variation of the efficiency was found to decrease from 4% at p_t = 1–2 GeV/c to less than 1% for $p_t > 5$ GeV/c. This effect was not included explicitly in the uncertainty estimation, since it is to some extent accounted for in the cut variation study and its magnitude is much smaller than the 10% uncertainty assigned to the cut efficiency corrections.

The systematic uncertainty induced by a different efficiency for particle identification in data and simulation was evaluated by repeating the analysis either without applying this selection, or with a tighter selection ($2\,\sigma$ compatibility instead of $3\,\sigma$). The variation of the

JHEP01(2012)128

corrected yields obtained without PID and with these two selections (standard and tighter) was assigned as a systematic uncertainty. Typical values are 3–5%, with the exception of 15% for D^+ in 1–2 GeV/c.

The accuracy of the description of the evolution of the experimental conditions with time was verified by analyzing separately sub-samples of data collected during different periods and with different orientations of the magnetic field. The results were found to be compatible within statistical uncertainties for all three meson species. Furthermore, the p_{t}-differential yields for each D meson measured separately for particles and anti-particles were found to be in agreement within statistical uncertainties.

The effect of the shape of the simulated D mesons spectrum within our p_{t} intervals was estimated from the relative difference in the Monte Carlo efficiencies obtained with the p_{t} shapes from PYTHIA [22] with Perugia-0 tune [23] and from the FONLL pQCD calculation [1, 2, 33]. These two models predict a significantly different slope at high p_{t} ($\mathrm{d}N/\mathrm{d}p_{\mathrm{t}} \propto p_{\mathrm{t}}^{-4.8}$ for FONLL and $\propto p_{\mathrm{t}}^{-2.5}$ for PYTHIA Perugia-0), which however results in a systematic effect on the D meson selection efficiency of only 3% for $1 < p_{\mathrm{t}} < 2$ GeV/c, and less than 1% at higher p_{t}.

The systematic uncertainty from the subtraction of feed-down D mesons from B decays was estimated as described in the previous section. It ranges between $^{+\,5}_{-45}$% at low p_{t} (1–2 GeV/c) and $^{+\,8}_{-10}$% at high p_{t} (> 12 GeV/c).

Finally, the results have global systematic uncertainties caused by the branching ratios (taken from [24]) and by the minimum-bias cross section (3.5%).

4.3 Results

The p_{t}-differential inclusive cross sections are shown in figure 5 for prompt D^0, D^+, and D^{*+} mesons. The error bars represent the statistical uncertainties, while the systematic uncertainties are shown as boxes around the data points. The numerical values for the differential cross sections are reported in table 3, together with their statistical and systematic uncertainties, as well as the average transverse momentum $\langle p_{\mathrm{t}} \rangle$ of D mesons in each p_{t} interval. The value of $\langle p_{\mathrm{t}} \rangle$ was obtained from the meson p_{t} distribution in the considered interval, after subtracting the background contribution from the side bands in the invariant mass distribution. The resulting $\langle p_{\mathrm{t}} \rangle$ values for the three D meson species are compatible within uncertainties in all p_{t} bins and their average is reported in the table.

The measured D meson inclusive differential production cross sections are compared to two theoretical predictions, namely FONLL [1, 2, 33] and GM-VFNS [10, 34]. Both calculations use CTEQ6.6 parton distribution functions (PDF) [35] and vary the factorization and renormalization scales, μ_{F} and μ_{R}, independently in the ranges $0.5 < \mu_{\mathrm{F}}/m_{\mathrm{t}} < 2$, $0.5 < \mu_{\mathrm{R}}/m_{\mathrm{t}} < 2$, with the constraint $0.5 < \mu_{\mathrm{F}}/\mu_{\mathrm{R}} < 2$, where $m_{\mathrm{t}} = \sqrt{p_{\mathrm{t}}^2 + m_{\mathrm{c}}^2}$. The charm quark mass is varied in FONLL within $1.3 < m_{\mathrm{c}} < 1.7$ GeV/c^2. Both calculations are compatible with the measurements, within the uncertainties. The central value of the GM-VFNS predictions lies systematically above the data, while that of the FONLL predictions lies below the data. For FONLL, this feature was observed also at $\sqrt{s} = 0.2$ TeV (pp) [11–13] and 1.96 TeV ($\mathrm{p\overline{p}}$) [8]. With a reach down to $p_{\mathrm{t}} = 1$ GeV/c, this measurement probes the gluon distribution in the x range of a few 10^{-4}. Within the current uncertainties

JHEP01(2012)128

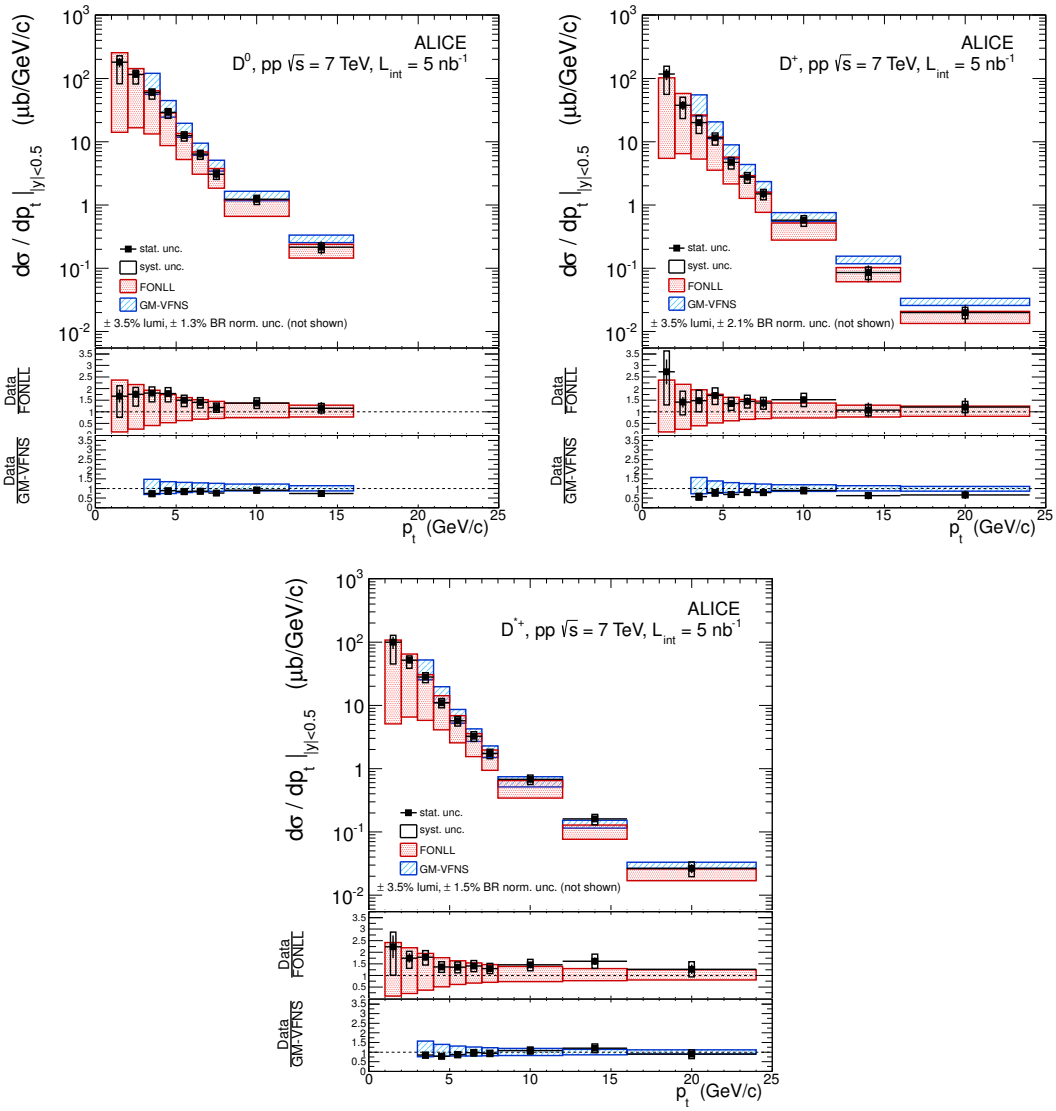

Figure 5. (colour online) $p_{\rm t}$-differential inclusive cross section for prompt $\rm D^0$, $\rm D^+$, and $\rm D^{*+}$ mesons in pp collisions at $\sqrt{s} = 7$ TeV compared with FONLL [1, 2, 33] and GM-VFNS [10, 34] theoretical predictions. The symbols are positioned horizontally at the centre of each $p_{\rm t}$ interval. The normalization uncertainty is not shown (3.5% from the minimum-bias cross section plus the branching ratio uncertainties, as of table 2).

of the experimental measurement and of the theoretical predictions, it is not possible to draw conclusions about small-x gluon saturation effects (see section 1).

The $p_{\rm t}$-integrated visible cross sections, $\sigma^{\rm vis}(p_{\rm t} > 1\ {\rm GeV}/c, |y| < 0.5)$, for the three mesons were extrapolated down to $p_{\rm t} = 0$ to estimate the production cross sections per unit of rapidity $\rm d\sigma/dy$ at mid-rapidity. The extrapolation factor was computed from the FONLL calculation [1, 2, 30] as the ratio $(\rm d\sigma_{FONLL}/dy)/\sigma^{vis}_{FONLL}$ and it amounts to $1.25^{+0.29}_{-0.09}$ for $\rm D^0$ and $\rm D^+$, and $1.21^{+0.29}_{-0.08}$ for $\rm D^{*+}$, for the central values of the calculation. Its uncertainty

JHEP01(2012)128

p_t interval	$\langle p_t \rangle$	$d\sigma/dp_t\|_{\|y\|<0.5}$ $\pm$ stat. $\pm$ syst. (μb/GeV/c)		
(GeV/c)	(GeV/c)	D^0	D^+	D^{*+}
1–2	1.5 ± 0.3	$180 \pm 30^{+48}_{-98}$	$117 \pm 23^{+39}_{-61}$	$100 \pm 22^{+28}_{-55}$
2–3	2.5 ± 0.2	$115 \pm 11^{+20}_{-33}$	$37.7 \pm 6.1^{+12.6}_{-14.5}$	$51.8 \pm 5.9^{+\ 8.7}_{-13.2}$
3–4	3.5 ± 0.1	$59.7 \pm 4.3^{+\ 8.5}_{-12.6}$	$20.1 \pm 2.2^{+6.0}_{-6.5}$	$28.0 \pm 2.3^{+4.6}_{-5.2}$
4–5	4.5 ± 0.1	$29.1 \pm 2.1^{+4.2}_{-5.8}$	$11.51 \pm 0.96^{+2.20}_{-2.64}$	$11.01 \pm 0.87^{+1.82}_{-1.88}$
5–6	5.5 ± 0.1	$12.5 \pm 1.1^{+1.8}_{-2.3}$	$4.72 \pm 0.47^{+0.92}_{-1.00}$	$5.70 \pm 0.45^{+0.97}_{-1.00}$
6–7	6.5 ± 0.1	$6.37 \pm 0.70^{+0.94}_{-1.08}$	$2.76 \pm 0.32^{+0.49}_{-0.55}$	$3.26 \pm 0.27^{+0.55}_{-0.57}$
7–8	7.4 ± 0.1	$3.07 \pm 0.47^{+0.50}_{-0.53}$	$1.50 \pm 0.22^{+0.27}_{-0.29}$	$1.74 \pm 0.21^{+0.30}_{-0.30}$
8–12	9.4 ± 0.3	$1.23 \pm 0.13^{+0.19}_{-0.21}$	$0.575 \pm 0.056^{+0.103}_{-0.115}$	$0.677 \pm 0.050^{+0.113}_{-0.116}$
12–16	13.8 ± 0.9	$0.215 \pm 0.050^{+0.037}_{-0.038}$	$0.085 \pm 0.026^{+0.019}_{-0.020}$	$0.160 \pm 0.016^{+0.030}_{-0.031}$
16–24	$17.0^{+2.0}_{-1.0}$	—	$0.020 \pm 0.007^{+0.004}_{-0.004}$	$0.027 \pm 0.004^{+0.007}_{-0.007}$

Table 3. Production cross section in $|y| < 0.5$ for prompt D^0, D^+, and D^{*+} mesons in pp collisions at $\sqrt{s} = 7$ TeV, in transverse momentum intervals. The normalization systematic uncertainty (3.5% from the minimum-bias cross section plus the branching ratio uncertainties, as of table 2) is not included in the systematic uncertainties reported in the table.

was obtained as a quadratic sum of the uncertainties from charm mass and perturbative scales, varied within the aforementioned ranges,[1] and from the CTEQ6.6 PDF sets [35]. The cross sections for the three mesons are:

$$d\sigma^{D^0}/dy = 516 \pm 41(\text{stat.})^{+\ 69}_{-175}(\text{syst.}) \pm 18(\text{lumi.}) \pm 7(\text{BR})^{+120}_{-\ 37}(\text{extr.})\ \mu\text{b},$$

$$d\sigma^{D^+}/dy = 248 \pm 30(\text{stat.})^{+52}_{-92}(\text{syst.}) \pm 9(\text{lumi.}) \pm 5(\text{BR})^{+57}_{-18}(\text{extr.})\ \mu\text{b},$$

$$d\sigma^{D^{*+}}/dy = 247 \pm 27(\text{stat.})^{+36}_{-81}(\text{syst.}) \pm 9(\text{lumi.}) \pm 4(\text{BR})^{+57}_{-16}(\text{extr.})\ \mu\text{b}.$$

5 Summary

We have presented the measurement by the ALICE Collaboration of the inclusive differential production cross sections of prompt D mesons at central rapidity, in pp collisions at $\sqrt{s} = 7$ TeV within $1 < p_t < 24$ GeV/c. D mesons were reconstructed in the decay channels $D^0 \to K^-\pi^+$, $D^+ \to K^-\pi^+\pi^+$, and $D^{*+} \to D^0\pi^+$, and their charge conjugates.

The p_t-differential cross sections are reproduced within uncertainties by theoretical predictions based on perturbative QCD, FONLL [33] and GM-VFNS [34]. More in detail, the data tend to be higher than the central value of the FONLL predictions, as it was observed also at lower collision energies, at RHIC and at the Tevatron [8, 11–13]. For

[1] The +0.29 (i.e. +23%) uncertainty is mainly determined by the case $\mu_F = 0.5\, m_t$, for which the PDFs are used in the region $Q \approx 0.5\, m_c$ that is not constrained by experimental data [35]. If this case is not considered, the uncertainty becomes +13% on the upper side.

JHEP01(2012)128

GM-VFNS, instead, the data lie on the lower side of the predictions, at variance with the case of Tevatron energy [8, 10], indicating that the energy dependence is steeper in this model than in data. Our results, together with existing measurements at lower energies, can contribute to a better understanding of charm production in pQCD.

Furthermore, the measurements that we have presented open new possibilities to test PDF dynamics, in the regime of parton fractional momentum below $x \sim 10^{-4}$ and squared momentum transfer down to $Q^2 \sim (4\ \mathrm{GeV})^2$, where the onset of gluon PDF saturation effects has been conjectured [14]. Within the uncertainties of the data and of the theoretical predictions, the framework of factorized QCD calculations provides a reasonable description of the data points down to the lowest measured transverse momentum. However, accurate calculations incorporating saturation effects are needed in order to draw firm conclusions on their relevance for low-momentum charm production at LHC energies.

Acknowledgments

The ALICE collaboration would like to thank all its engineers and technicians for their invaluable contributions to the construction of the experiment and the CERN accelerator teams for the outstanding performance of the LHC complex. The ALICE Collaboration would like to thank M. Cacciari and H. Spiesberger for providing the pQCD predictions that are compared to these data. The ALICE collaboration acknowledges the following funding agencies for their support in building and running the ALICE detector: Department of Science and Technology, South Africa; Calouste Gulbenkian Foundation from Lisbon and Swiss Fonds Kidagan, Armenia; Conselho Nacional de Desenvolvimento Científico e Tecnológico (CNPq), Financiadora de Estudos e Projetos (FINEP), Fundação de Amparo à Pesquisa do Estado de São Paulo (FAPESP); National Natural Science Foundation of China (NSFC), the Chinese Ministry of Education (CMOE) and the Ministry of Science and Technology of China (MSTC); Ministry of Education and Youth of the Czech Republic; Danish Natural Science Research Council, the Carlsberg Foundation and the Danish National Research Foundation; The European Research Council under the European Community's Seventh Framework Programme; Helsinki Institute of Physics and the Academy of Finland; French CNRS-IN2P3, the 'Region Pays de Loire', 'Region Alsace', 'Region Auvergne' and CEA, France; German BMBF and the Helmholtz Association; General Secretariat for Research and Technology, Ministry of Development, Greece; Hungarian OTKA and National Office for Research and Technology (NKTH); Department of Atomic Energy and Department of Science and Technology of the Government of India; Istituto Nazionale di Fisica Nucleare (INFN) of Italy; MEXT Grant-in-Aid for Specially Promoted Research, Japan; Joint Institute for Nuclear Research, Dubna; National Research Foundation of Korea (NRF); CONACYT, DGAPA, México, ALFA-EC and the HELEN Program (High-Energy physics Latin-American–European Network); Stichting voor Fundamenteel Onderzoek der Materie (FOM) and the Nederlandse Organisatie voor Wetenschappelijk Onderzoek (NWO), Netherlands; Research Council of Norway (NFR); Polish Ministry of Science and Higher Education; National Authority for Scientific Research - NASR (Autoritatea Naţională pentru Cercetare Ştiinţifică - ANCS); Federal Agency of Science of

JHEP01(2012)128

the Ministry of Education and Science of Russian Federation, International Science and Technology Center, Russian Academy of Sciences, Russian Federal Agency of Atomic Energy, Russian Federal Agency for Science and Innovations and CERN-INTAS; Ministry of Education of Slovakia; CIEMAT, EELA, Ministerio de Educación y Ciencia of Spain, Xunta de Galicia (Consellería de Educación), CEADEN, Cubaenergía, Cuba, and IAEA (International Atomic Energy Agency); Swedish Reseach Council (VR) and Knut & Alice Wallenberg Foundation (KAW); Ukraine Ministry of Education and Science; United Kingdom Science and Technology Facilities Council (STFC); The United States Department of Energy, the United States National Science Foundation, the State of Texas, and the State of Ohio.

References

[1] M. Cacciari, M. Greco and P. Nason, *The p_T spectrum in heavy flavor hadroproduction*, *JHEP* **05** (1998) 007 [hep-ph/9803400] [INSPIRE].

[2] M. Cacciari, S. Frixione and P. Nason, *The p_T spectrum in heavy flavor photoproduction*, *JHEP* **03** (2001) 006 [hep-ph/0102134] [INSPIRE].

[3] CDF collaboration, D. Acosta et al., *Measurement of the J/ψ meson and b-hadron production cross sections in $p\bar{p}$ collisions at $\sqrt{s} = 1960$ GeV*, *Phys. Rev.* **D 71** (2005) 032001 [hep-ex/0412071] [INSPIRE].

[4] M. Cacciari, S. Frixione, M. Mangano, P. Nason and G. Ridolfi, *QCD analysis of first b cross-section data at 1.96 TeV*, *JHEP* **07** (2004) 033 [hep-ph/0312132] [INSPIRE].

[5] B.A. Kniehl, G. Kramer, I. Schienbein and H. Spiesberger, *Finite-mass effects on inclusive B meson hadroproduction*, *Phys. Rev.* **D 77** (2008) 014011 [arXiv:0705.4392] [INSPIRE].

[6] LHCb collaboration, R. Aaij et al., *Measurement of $\sigma(pp \to b\bar{b}X)$ at $\sqrt{s} = 7$ TeV in the forward region*, *Phys. Lett.* **B 694** (2010) 209 [arXiv:1009.2731] [INSPIRE].

[7] CMS collaboration, V. Khachatryan et al., *Prompt and non-prompt J/ψ production in pp collisions at $\sqrt{s} = 7$ TeV*, *Eur. Phys. J.* **C 71** (2011) 1575 [arXiv:1011.4193] [INSPIRE].

[8] CDF collaboration, D. Acosta et al., *Measurement of prompt charm meson production cross sections in $p\bar{p}$ collisions at $\sqrt{s} = 1.96$ TeV*, *Phys. Rev. Lett.* **91** (2003) 241804 [hep-ex/0307080] [INSPIRE].

[9] M. Cacciari and P. Nason, *Charm cross-sections for the Tevatron Run II*, *JHEP* **09** (2003) 006 [hep-ph/0306212] [INSPIRE].

[10] B. Kniehl, G. Kramer, I. Schienbein and H. Spiesberger, *Reconciling open charm production at the Fermilab Tevatron with QCD*, *Phys. Rev. Lett.* **96** (2006) 012001 [hep-ph/0508129] [INSPIRE].

[11] PHENIX collaboration, A. Adare et al., *Measurement of high-p_T single electrons from heavy-flavor decays in $p+p$ collisions at $\sqrt{s} = 200$ GeV*, *Phys. Rev. Lett.* **97** (2006) 252002 [hep-ex/0609010] [INSPIRE].

JHEP01(2012)128

[12] STAR collaboration, B. Abelev et al., *Transverse momentum and centrality dependence of high-p_T non-photonic electron suppression in Au+Au collisions at $\sqrt{s_{NN}} = 200$ GeV*, *Phys. Rev. Lett.* **98** (2007) 192301 [*Erratum ibid.* **106** (2011) 159902] [nucl-ex/0607012] [INSPIRE].

[13] STAR collaboration, W. Xie et al., *Measurement of open heavy flavor production in the STAR experiment at RHIC*, PoS(DIS 2010)182.

[14] S. Alekhin et al., *HERA and the LHC: A Workshop on the implications of HERA for LHC physics. Proceedings, Part B*, hep-ph/0601013, see chapter IV [INSPIRE].

[15] ALICE collaboration, K. Aamodt et al., *The ALICE experiment at the CERN LHC*, 2008 *JINST* **3** S08002 [INSPIRE].

[16] ALICE collaboration, K. Aamodt et al., *Alignment of the ALICE inner tracking system with cosmic-ray tracks*, 2010 *JINST* **5** P03003 [arXiv:1001.0502] [INSPIRE].

[17] ALICE collaboration, A. Rossi et al., *ALICE alignment, tracking and physics performance results*, PoS(VERTEX 2010)017 [arXiv:1101.3491] [INSPIRE].

[18] J. Alme et al., *The ALICE TPC, a large 3-dimensional tracking device with fast readout for ultra-high multiplicity events*, *Nucl. Instrum. Meth.* **A 622** (2010) 316 [arXiv:1001.1950] [INSPIRE].

[19] A. Akindinov et al., *The commissioning of the ALICE time-of-flight detector and results from the 2008 cosmic-ray data taking*, *Nucl. Instrum. Meth.* **A 615** (2010) 37 [INSPIRE].

[20] ALICE collaboration, M. Gagliardi et al., *Measurement of reference cross sections in pp and Pb-Pb collisions at the LHC in van der Meer scans with the ALICE detector*, arXiv:1109.5369 [INSPIRE].

[21] ALICE collaboration, *Measurement of inelastic, single and double diffractive cross sections in proton–proton collisions at the LHC with ALICE*, in preparation.

[22] T. Sjöstrand, S. Mrenna and P.Z. Skands, *PYTHIA 6.4 physics and manual*, *JHEP* **05** (2006) 026 [hep-ph/0603175] [INSPIRE].

[23] P.Z. Skands, *The Perugia tunes*, arXiv:0905.3418 [INSPIRE].

[24] Particle Data Group collaboration, K. Nakamura et al., *Review of particle physics*, *J. Phys.* **G 37** (2010) 075021 [INSPIRE].

[25] ALICE collaboration, K. Aamodt et al., *Production of pions, kaons and protons in pp collisions at $\sqrt{s} = 900$ GeV with ALICE at the LHC*, *Eur. Phys. J.* **C 71** (2011) 1655 [arXiv:1101.4110] [INSPIRE].

[26] E. Bruna et al., *Vertex reconstruction for proton-proton collisions in ALICE*, ALICE-INT-2009-018 (2009).

[27] R. Brun et al., *CERN program library long write-up, W5013, GEANT detector description and simulation tool* (1994).

[28] S. van der Meer, *Calibration of the effective beam height in the ISR*, CERN-ISR-PO-68-31 [ISR-PO-68-31].

[29] G. Anders et al., *LHC bunch current normalisation for the october 2010 luminosity calibration measurements*, ATS-Note-2011-016 (2011).

[30] M. Cacciari, private communication.

[31] D. Lange, *The EvtGen particle decay simulation package*, *Nucl. Instrum. Meth.* **A 462** (2001) 152 [INSPIRE].

JHEP01(2012)128

[32] M. Cacciari, P. Nason and R. Vogt, *QCD predictions for charm and bottom production at RHIC*, *Phys. Rev. Lett.* **95** (2005) 122001 [hep-ph/0502203] [INSPIRE].

[33] M. Cacciari et al., *Theoretical predictions for charm and bottom production at the LHC*, CERN-PH-TH-2011-227 (2011).

[34] B.A. Kniehl, G. Kramer, I. Schienbein and H. Spiesberger, in preparation.

[35] P.M. Nadolsky et al., *Implications of CTEQ global analysis for collider observables*, *Phys. Rev.* **D 78** (2008) 013004 [arXiv:0802.0007] [INSPIRE].

JHEP01(2012)128

The ALICE collaboration

B. Abelev[69] , A. Abrahantes Quintana[6] , D. Adamová[74] , A.M. Adare[120] , M.M. Aggarwal[78] , G. Aglieri Rinella[30] , A.G. Agocs[60] , A. Agostinelli[19] , S. Aguilar Salazar[56] , Z. Ahammed[116] , N. Ahmad[14] , A. Ahmad Masoodi[14] , S.U. Ahn[64,37] , A. Akindinov[46] , D. Aleksandrov[89] , B. Alessandro[95] , R. Alfaro Molina[56] , A. Alici[96,30,9] , A. Alkin[2] , E. Almaráz Aviña[56] , T. Alt[36] , V. Altini[28,30] , S. Altinpinar[15] , I. Altsybeev[117] , C. Andrei[71] , A. Andronic[86] , V. Anguelov[83] , C. Anson[16] , T. Antičić[87] , F. Antinori[100] , P. Antonioli[96] , L. Aphecetche[102] , H. Appelshäuser[52] , N. Arbor[65] , S. Arcelli[19] , A. Arend[52] , N. Armesto[13] , R. Arnaldi[95] , T. Aronsson[120] , I.C. Arsene[86] , M. Arslandok[52] , A. Asryan[117] , A. Augustinus[30] , R. Averbeck[86] , T.C. Awes[75] , J. Äystö[38] , M.D. Azmi[14] , M. Bach[36] , A. Badalà[97] , Y.W. Baek[64,37] , R. Bailhache[52] , R. Bala[95] , R. Baldini Ferroli[9] , A. Baldisseri[12] , A. Baldit[64] , F. Baltasar Dos Santos Pedrosa[30] , J. Bán[47] , R.C. Baral[48] , R. Barbera[24] , F. Barile[28] , G.G. Barnaföldi[60] , L.S. Barnby[91] , V. Barret[64] , J. Bartke[104] , M. Basile[19] , N. Bastid[64] , B. Bathen[54] , G. Batigne[102] , B. Batyunya[59] , C. Baumann[52] , I.G. Bearden[72] , H. Beck[52] , I. Belikov[58] , F. Bellini[19] , R. Bellwied[110] , E. Belmont-Moreno[56] , S. Beole[26] , I. Berceanu[71] , A. Bercuci[71] , Y. Berdnikov[76] , D. Berenyi[60] , C. Bergmann[54] , D. Berzano[26] , L. Betev[30] , A. Bhasin[81] , A.K. Bhati[78] , N. Bianchi[66] , L. Bianchi[26] , C. Bianchin[22] , J. Bielčík[34] , J. Bielčíková[74] , A. Bilandzic[73] , F. Blanco[110] , F. Blanco[7] , D. Blau[89] , C. Blume[52] , M. Boccioli[30] , N. Bock[16] , A. Bogdanov[70] , H. Bøggild[72] , M. Bogolyubsky[43] , L. Boldizsár[60] , M. Bombara[35] , J. Book[52] , H. Borel[12] , A. Borissov[119] , C. Bortolin[22,ii], S. Bose[90] , F. Bossú[30,26] , M. Botje[73] , S. Böttger[51] , B. Boyer[42] , P. Braun-Munzinger[86] , M. Bregant[102] , T. Breitner[51] , M. Broz[33] , R. Brun[30] , E. Bruna[120,26,95] , G.E. Bruno[28] , D. Budnikov[88] , H. Buesching[52] , S. Bufalino[26,95] , K. Bugaiev[2] , O. Busch[83] , Z. Buthelezi[80] , D. Caffarri[22] , X. Cai[40] , H. Caines[120] , E. Calvo Villar[92] , P. Camerini[20] , V. Canoa Roman[8,1] , G. Cara Romeo[96] , W. Carena[30] , F. Carena[30] , N. Carlin Filho[107] , F. Carminati[30] , C.A. Carrillo Montoya[30] , A. Casanova Díaz[66] , M. Caselle[30] , J. Castillo Castellanos[12] , J.F. Castillo Hernandez[86] , E.A.R. Casula[21] , V. Catanescu[71] , C. Cavicchioli[30] , J. Cepila[34] , P. Cerello[95] , B. Chang[38,123] , S. Chapeland[30] , J.L. Charvet[12] , S. Chattopadhyay[90] , S. Chattopadhyay[116] , M. Cherney[77] , C. Cheshkov[30,109] , B. Cheynis[109] , E. Chiavassa[95] , V. Chibante Barroso[30] , D.D. Chinellato[108] , P. Chochula[30] , M. Chojnacki[45] , P. Christakoglou[73,45] , C.H. Christensen[72] , P. Christiansen[29] , T. Chujo[114] , S.U. Chung[85] , C. Cicalo[93] , L. Cifarelli[19,30] , F. Cindolo[96] , J. Cleymans[80] , F. Coccetti[9] , J.-P. Coffin[58] , F. Colamaria[28] , D. Colella[28] , G. Conesa Balbastre[65] , Z. Conesa del Valle[30,58] , P. Constantin[83] , G. Contin[20] , J.G. Contreras[8] , T.M. Cormier[119] , Y. Corrales Morales[26] , P. Cortese[27] , I. Cortés Maldonado[1] , M.R. Cosentino[68,108] , F. Costa[30] , M.E. Cotallo[7] , E. Crescio[8] , P. Crochet[64] , E. Cruz Alaniz[56] , E. Cuautle[55] , L. Cunqueiro[66] , A. Dainese[100] , H.H. Dalsgaard[72] , A. Danu[50] , D. Das[90] , I. Das[90] , K. Das[90] , S. Dash[95] , A. Dash[48,108] , S. De[116] , A. De Azevedo Moregula[66] , G.O.V. de Barros[107] , A. De Caro[25,9] , G. de Cataldo[94] , J. de Cuveland[36] ,

JHEP01(2012)128

A. De Falco[21] , D. De Gruttola[25] , H. Delagrange[102] , E. Del Castillo Sanchez[30] , A. Deloff[101] , V. Demanov[88] , N. De Marco[95] , E. Dénes[60] , S. De Pasquale[25] , A. Deppman[107] , G. D Erasmo[28] , R. de Rooij[45] , D. Di Bari[28] , T. Dietel[54] , C. Di Giglio[28] , S. Di Liberto[99] , A. Di Mauro[30] , P. Di Nezza[66] , R. Divià[30] , Ø. Djuvsland[15] , A. Dobrin[119 ,29] , T. Dobrowolski[101] , I. Domínguez[55] , B. Dönigus[86] , O. Dordic[18] , O. Driga[102] , A.K. Dubey[116] , L. Ducroux[109] , P. Dupieux[64] , M.R. Dutta Majumdar[116] , A.K. Dutta Majumdar[90] , D. Elia[94] , D. Emschermann[54] , H. Engel[51] , H.A. Erdal[32] , B. Espagnon[42] , M. Estienne[102] , S. Esumi[114] , D. Evans[91] , G. Eyyubova[18] , D. Fabris[22 ,100] , J. Faivre[65] , D. Falchieri[19] , A. Fantoni[66] , M. Fasel[86] , R. Fearick[80] , A. Fedunov[59] , D. Fehlker[15] , L. Feldkamp[54] , D. Felea[50] , G. Feofilov[117] , A. Fernández Téllez[1] , A. Ferretti[26] , R. Ferretti[27] , J. Figiel[104] , M.A.S. Figueredo[107] , S. Filchagin[88] , R. Fini[94] , D. Finogeev[44] , F.M. Fionda[28] , E.M. Fiore[28] , M. Floris[30] , S. Foertsch[80] , P. Foka[86] , S. Fokin[89] , E. Fragiacomo[98] , M. Fragkiadakis[79] , U. Frankenfeld[86] , U. Fuchs[30] , C. Furget[65] , M. Fusco Girard[25] , J.J. Gaardhøje[72] , M. Gagliardi[26] , A. Gago[92] , M. Gallio[26] , D.R. Gangadharan[16] , P. Ganoti[75] , C. Garabatos[86] , E. Garcia-Solis[10] , I. Garishvili[69] , J. Gerhard[36] , M. Germain[102] , C. Geuna[12] , A. Gheata[30] , M. Gheata[30] , B. Ghidini[28] , P. Ghosh[116] , P. Gianotti[66] , M.R. Girard[118] , P. Giubellino[30 ,26] , E. Gladysz-Dziadus[104] , P. Glässel[83] , R. Gomez[106] , E.G. Ferreiro[13] , L.H. González-Trueba[56] , P. González-Zamora[7] , S. Gorbunov[36] , A. Goswami[82] , S. Gotovac[103] , V. Grabski[56] , L.K. Graczykowski[118] , R. Grajcarek[83] , A. Grelli[45] , A. Grigoras[30] , C. Grigoras[30] , V. Grigoriev[70] , S. Grigoryan[59] , A. Grigoryan[121] , B. Grinyov[2] , N. Grion[98] , P. Gros[29] , J.F. Grosse-Oetringhaus[30] , J.-Y. Grossiord[109] , R. Grosso[30] , F. Guber[44] , R. Guernane[65] , C. Guerra Gutierrez[92] , B. Guerzoni[19] , M. Guilbaud[109] , K. Gulbrandsen[72] , T. Gunji[113] , A. Gupta[81] , R. Gupta[81] , H. Gutbrod[86] , Ø. Haaland[15] , C. Hadjidakis[42] , M. Haiduc[50] , H. Hamagaki[113] , G. Hamar[60] , B.H. Han[17] , L.D. Hanratty[91] , A. Hansen[72] , Z. Harmanova[35] , J.W. Harris[120] , M. Hartig[52] , D. Hasegan[50] , D. Hatzifotiadou[96] , A. Hayrapetyan[30 ,121] , M. Heide[54] , H. Helstrup[32] , A. Herghelegiu[71] , G. Herrera Corral[8] , N. Herrmann[83] , K.F. Hetland[32] , B. Hicks[120] , P.T. Hille[120] , B. Hippolyte[58] , T. Horaguchi[114] , Y. Hori[113] , P. Hristov[30] , I. Hřivnáčová[42] , M. Huang[15] , S. Huber[86] , T.J. Humanic[16] , D.S. Hwang[17] , R. Ichou[64] , R. Ilkaev[88] , I. Ilkiv[101] , M. Inaba[114] , E. Incani[21] , P.G. Innocenti[30] , G.M. Innocenti[26] , M. Ippolitov[89] , M. Irfan[14] , C. Ivan[86] , A. Ivanov[117] , M. Ivanov[86] , V. Ivanov[76] , O. Ivanytskyi[2] , A. Jachołkowski[30] , P. M. Jacobs[68] , L. Jancurová[59] , S. Jangal[58] , M.A. Janik[118] , R. Janik[33] , P.H.S.Y. Jayarathna[110] , S. Jena[41] , R.T. Jimenez Bustamante[55] , L. Jirden[30] , P.G. Jones[91] , H. Jung[37] , W. Jung[37] , A. Jusko[91] , A.B. Kaidalov[46] , V. Kakoyan[121] , S. Kalcher[36] , P. Kaliňák[47] , M. Kalisky[54] , T. Kalliokoski[38] , A. Kalweit[53] , K. Kanaki[15] , J.H. Kang[123] , V. Kaplin[70] , A. Karasu Uysal[30 ,122] , O. Karavichev[44] , T. Karavicheva[44] , E. Karpechev[44] , A. Kazantsev[89] , U. Kebschull[62 ,51] , R. Keidel[124] , M.M. Khan[14] , S.A. Khan[116] , P. Khan[90] , A. Khanzadeev[76] , Y. Kharlov[43] , B. Kileng[32] , S. Kim[17] , D.W. Kim[37] , J.H. Kim[17] , J.S. Kim[37] , M. Kim[123] , S.H. Kim[37] , T. Kim[123] , B. Kim[123] , D.J. Kim[38] , S. Kirsch[36 ,30] , I. Kisel[36] , S. Kiselev[46] , A. Kisiel[30 ,118] , J.L. Klay[4] , J. Klein[83] ,

JHEP01(2012)128

C. Klein-Bösing[54] , M. Kliemant[52] , A. Kluge[30] , M.L. Knichel[86] , K. Koch[83] , M.K. Köhler[86] , A. Kolojvari[117] , V. Kondratiev[117] , N. Kondratyeva[70] , A. Konevskikh[44] , C. Kottachchi Kankanamge Don[119] , R. Kour[91] , M. Kowalski[104] , S. Kox[65] , G. Koyithatta Meethaleveedu[41] , J. Kral[38] , I. Králik[47] , F. Kramer[52] , I. Kraus[86] , T. Krawutschke[83,31] , M. Kretz[36] , M. Krivda[91,47] , F. Krizek[38] , M. Krus[34] , E. Kryshen[76] , M. Krzewicki[73] , Y. Kucheriaev[89] , C. Kuhn[58] , P.G. Kuijer[73] , P. Kurashvili[101] , A.B. Kurepin[44] , A. Kurepin[44] , A. Kuryakin[88] , V. Kushpil[74] , S. Kushpil[74] , H. Kvaerno[18] , M.J. Kweon[83] , Y. Kwon[123] , P. Ladrón de Guevara[55] , I. Lakomov[117] , R. Langoy[15] , C. Lara[51] , A. Lardeux[102] , P. La Rocca[24] , D.T. Larsen[15] , C. Lazzeroni[91] , R. Lea[20] , Y. Le Bornec[42] , S.C. Lee[37] , K.S. Lee[37] , F. Lefèvre[102] , J. Lehnert[52] , L. Leistam[30] , M. Lenhardt[102] , V. Lenti[94] , H. León[56] , I. León Monzón[106] , H. León Vargas[52] , P. Lévai[60] , X. Li[11] , J. Lien[15] , R. Lietava[91] , S. Lindal[18] , V. Lindenstruth[36] , C. Lippmann[86,30] , M.A. Lisa[16] , L. Liu[15] , P.I. Loenne[15] , V.R. Loggins[119] , V. Loginov[70] , S. Lohn[30] , D. Lohner[83] , C. Loizides[68] , K.K. Loo[38] , X. Lopez[64] , E. López Torres[6] , G. Løvhøiden[18] , X.-G. Lu[83] , P. Luettig[52] , M. Lunardon[22] , J. Luo[40] , G. Luparello[45] , L. Luquin[102] , C. Luzzi[30] , R. Ma[120] , K. Ma[40] , D.M. Madagodahettige-Don[110] , A. Maevskaya[44] , M. Mager[53,30] , D.P. Mahapatra[48] , A. Maire[58] , M. Malaev[76] , I. Maldonado Cervantes[55] , L. Malinina[59,,iii], D. Mal'Kevich[46] , P. Malzacher[86] , A. Mamonov[88] , L. Manceau[95] , L. Mangotra[81] , V. Manko[89] , F. Manso[64] , V. Manzari[94] , Y. Mao[65,40] , M. Marchisone[64,26] , J. Mareš[49] , G.V. Margagliotti[20,98] , A. Margotti[96] , A. Marín[86] , C. Markert[105] , I. Martashvili[112] , P. Martinengo[30] , M.I. Martínez[1] , A. Martínez Davalos[56] , G. Martínez García[102] , Y. Martynov[2] , A. Mas[102] , S. Masciocchi[86] , M. Masera[26] , A. Masoni[93] , L. Massacrier[109] , M. Mastromarco[94] , A. Mastroserio[28,30] , Z.L. Matthews[91] , A. Matyja[104,102] , D. Mayani[55] , C. Mayer[104] , M.A. Mazzoni[99] , F. Meddi[23] , A. Menchaca-Rocha[56] , J. Mercado Pérez[83] , M. Meres[33] , Y. Miake[114] , A. Michalon[58] , J. Midori[39] , L. Milano[26] , J. Milosevic[18,,iv], A. Mischke[45] , A.N. Mishra[82] , D. Miśkowiec[86,30] , C. Mitu[50] , J. Mlynarz[119] , A.K. Mohanty[30] , B. Mohanty[116] , L. Molnar[30] , L. Montaño Zetina[8] , M. Monteno[95] , E. Montes[7] , T. Moon[123] , M. Morando[22] , D.A. Moreira De Godoy[107] , S. Moretto[22] , A. Morsch[30] , V. Muccifora[66] , E. Mudnic[103] , S. Muhuri[116] , H. Müller[30] , M.G. Munhoz[107] , L. Musa[30] , A. Musso[95] , B.K. Nandi[41] , R. Nania[96] , E. Nappi[94] , C. Nattrass[112] , N.P. Naumov[88] , S. Navin[91] , T.K. Nayak[116] , S. Nazarenko[88] , G. Nazarov[88] , A. Nedosekin[46] , M. Nicassio[28] , B.S. Nielsen[72] , T. Niida[114] , S. Nikolaev[89] , V. Nikolic[87] , V. Nikulin[76] , S. Nikulin[89] , B.S. Nilsen[77] , M.S. Nilsson[18] , F. Noferini[96,9] , P. Nomokonov[59] , G. Nooren[45] , N. Novitzky[38] , A. Nyanin[89] , A. Nyatha[41] , C. Nygaard[72] , J. Nystrand[15] , H. Obayashi[39] , A. Ochirov[117] , H. Oeschler[53,30] , S.K. Oh[37] , J. Oleniacz[118] , C. Oppedisano[95] , A. Ortiz Velasquez[55] , G. Ortona[30,26] , A. Oskarsson[29] , P. Ostrowski[118] , I. Otterlund[29] , J. Otwinowski[86] , K. Oyama[83] , K. Ozawa[113] , Y. Pachmayer[83] , M. Pachr[34] , F. Padilla[26] , P. Pagano[25] , G. Paić[55] , F. Painke[36] , C. Pajares[13] , S. Pal[12] , S.K. Pal[116] , A. Palaha[91] , A. Palmeri[97] , V. Papikyan[121] , G.S. Pappalardo[97] , W.J. Park[86] , A. Passfeld[54] , B. Pastirčák[47] , D.I. Patalakha[43] , V. Paticchio[94] , A. Pavlinov[119] , T. Pawlak[118] , T. Peitzmann[45] , M. Perales[10] ,

JHEP01(2012)128

E. Pereira De Oliveira Filho[107] , D. Peresunko[89] , C.E. Pérez Lara[73] , E. Perez Lezama[55] , D. Perini[30] , D. Perrino[28] , W. Peryt[118] , A. Pesci[96] , V. Peskov[30,55] , Y. Pestov[3] , V. Petráček[34] , M. Petran[34] , M. Petris[71] , P. Petrov[91] , M. Petrovici[71] , C. Petta[24] , S. Piano[98] , A. Piccotti[95] , M. Pikna[33] , P. Pillot[102] , O. Pinazza[30] , L. Pinsky[110] , N. Pitz[52] , F. Piuz[30] , D.B. Piyarathna[110] , M. Płoskoń[68] , J. Pluta[118] , T. Pocheptsov[59,18] , S. Pochybova[60] , P.L.M. Podesta-Lerma[106] , M.G. Poghosyan[30,26] , K. Polák[49] , B. Polichtchouk[43] , A. Pop[71] , S. Porteboeuf-Houssais[64] , V. Pospíšil[34] , B. Potukuchi[81] , S.K. Prasad[119] , R. Preghenella[96,9] , F. Prino[95] , C.A. Pruneau[119] , I. Pshenichnov[44] , G. Puddu[21] , A. Pulvirenti[24,30] , V. Punin[88] , M. Putiš[35] , J. Putschke[119,120] , E. Quercigh[30] , H. Qvigstad[18] , A. Rachevski[98] , A. Rademakers[30] , S. Radomski[83] , T.S. Räihä[38] , J. Rak[38] , A. Rakotozafindrabe[12] , L. Ramello[27] , A. Ramírez Reyes[8] , S. Raniwala[82] , R. Raniwala[82] , S.S. Räsänen[38] , B.T. Rascanu[52] , D. Rathee[78] , K.F. Read[112] , J.S. Real[65] , K. Redlich[101,57] , P. Reichelt[52] , M. Reicher[45] , R. Renfordt[52] , A.R. Reolon[66] , A. Reshetin[44] , F. Rettig[36] , J.-P. Revol[30] , K. Reygers[83] , H. Ricaud[53] , L. Riccati[95] , R.A. Ricci[67] , M. Richter[18] , P. Riedler[30] , W. Riegler[30] , F. Riggi[24,97] , M. Rodríguez Cahuantzi[1] , D. Rohr[36] , D. Röhrich[15] , R. Romita[86] , F. Ronchetti[66] , P. Rosnet[64] , S. Rossegger[30] , A. Rossi[22] , F. Roukoutakis[79] , C. Roy[58] , P. Roy[90] , A.J. Rubio Montero[7] , R. Rui[20] , E. Ryabinkin[89] , A. Rybicki[104] , S. Sadovsky[43] , K. Šafařík[30] , P.K. Sahu[48] , J. Saini[116] , H. Sakaguchi[39] , S. Sakai[68] , D. Sakata[114] , C.A. Salgado[13] , S. Sambyal[81] , V. Samsonov[76] , X. Sanchez Castro[55] , L. Šándor[47] , A. Sandoval[56] , M. Sano[114] , S. Sano[113] , R. Santo[54] , R. Santoro[94,30] , J. Sarkamo[38] , E. Scapparone[96] , F. Scarlassara[22] , R.P. Scharenberg[84] , C. Schiaua[71] , R. Schicker[83] , H.R. Schmidt[86,115] , C. Schmidt[86] , S. Schreiner[30] , S. Schuchmann[52] , J. Schukraft[30] , Y. Schutz[30,102] , K. Schwarz[86] , K. Schweda[86,83] , G. Scioli[19] , E. Scomparin[95] , R. Scott[112] , P.A. Scott[91] , G. Segato[22] , I. Selyuzhenkov[86] , S. Senyukov[27,58] , J. Seo[85] , S. Serci[21] , E. Serradilla[7,56] , A. Sevcenco[50] , I. Sgura[94] , G. Shabratova[59] , R. Shahoyan[30] , N. Sharma[78] , S. Sharma[81] , K. Shigaki[39] , M. Shimomura[114] , K. Shtejer[6] , Y. Sibiriak[89] , M. Siciliano[26] , E. Sicking[30] , S. Siddhanta[93] , T. Siemiarczuk[101] , D. Silvermyr[75] , G. Simonetti[28,30] , R. Singaraju[116] , R. Singh[81] , S. Singha[116] , T. Sinha[90] , B.C. Sinha[116] , B. Sitar[33] , M. Sitta[27] , T.B. Skaali[18] , K. Skjerdal[15] , R. Smakal[34] , N. Smirnov[120] , R. Snellings[45] , C. Søgaard[72] , R. Soltz[69] , H. Son[17] , J. Song[85] , M. Song[123] , C. Soos[30] , F. Soramel[22] , M. Spyropoulou-Stassinaki[79] , B.K. Srivastava[84] , J. Stachel[83] , I. Stan[50] , I. Stan[50] , G. Stefanek[101] , G. Stefanini[30] , T. Steinbeck[36] , M. Steinpreis[16] , E. Stenlund[29] , G. Steyn[80] , D. Stocco[102] , M. Stolpovskiy[43] , P. Strmen[33] , A.A.P. Suaide[107] , M.A. Subieta Vásquez[26] , T. Sugitate[39] , C. Suire[42] , M. Sukhorukov[88] , R. Sultanov[46] , M. Šumbera[74] , T. Susa[87] , A. Szanto de Toledo[107] , I. Szarka[33] , A. Szostak[15] , C. Tagridis[79] , J. Takahashi[108] , J.D. Tapia Takaki[42] , A. Tauro[30] , G. Tejeda Muñoz[1] , A. Telesca[30] , C. Terrevoli[28] , J. Thäder[86] , J.H. Thomas[86] , D. Thomas[45] , R. Tieulent[109] , A.R. Timmins[110] , D. Tlusty[34] , A. Toia[36,30] , H. Torii[39,113] , L. Toscano[95] , F. Tosello[95] , T. Traczyk[118] , D. Truesdale[16] , W.H. Trzaska[38] , T. Tsuji[113] , A. Tumkin[88] , R. Turrisi[100] , T.S. Tveter[18] , J. Ulery[52] , K. Ullaland[15] , J. Ulrich[62,51] , A. Uras[109] , J. Urbán[35] , G.M. Urciuoli[99] , G.L. Usai[21] , M. Vajzer[34,74] ,

JHEP01(2012)128

M. Vala[59,47], L. Valencia Palomo[42], S. Vallero[83], N. van der Kolk[73], P. Vande Vyvre[30], M. van Leeuwen[45], L. Vannucci[67], A. Vargas[1], R. Varma[41], M. Vasileiou[79], A. Vasiliev[89], V. Vechernin[117], M. Veldhoen[45], M. Venaruzzo[20], E. Vercellin[26], S. Vergara[1], D.C. Vernekohl[54], R. Vernet[5], M. Verweij[45], L. Vickovic[103], G. Viesti[22], O. Vikhlyantsev[88], Z. Vilakazi[80], O. Villalobos Baillie[91], A. Vinogradov[89], L. Vinogradov[117], Y. Vinogradov[88], T. Virgili[25], Y.P. Viyogi[116], A. Vodopyanov[59], K. Voloshin[46], S. Voloshin[119], G. Volpe[28,30], B. von Haller[30], D. Vranic[86], G. Øvrebekk[15], J. Vrláková[35], B. Vulpescu[64], A. Vyushin[88], V. Wagner[34], B. Wagner[15], R. Wan[58,40], Y. Wang[40], D. Wang[40], Y. Wang[83], M. Wang[40], K. Watanabe[114], J.P. Wessels[30,54], U. Westerhoff[54], J. Wiechula[83,115], J. Wikne[18], M. Wilde[54], G. Wilk[101], A. Wilk[54], M.C.S. Williams[96], B. Windelband[83], L. Xaplanteris Karampatsos[105], H. Yang[12], S. Yano[39], S. Yasnopolskiy[89], J. Yi[85], Z. Yin[40], H. Yokoyama[114], I.-K. Yoo[85], J. Yoon[123], W. Yu[52], X. Yuan[40], I. Yushmanov[89], C. Zach[34], C. Zampolli[96,30], S. Zaporozhets[59], A. Zarochentsev[117], P. Závada[49], N. Zaviyalov[88], H. Zbroszczyk[118], P. Zelnicek[30,51], I. Zgura[50], M. Zhalov[76], X. Zhang[64,40], F. Zhou[40], D. Zhou[40], Y. Zhou[45], X. Zhu[40], A. Zichichi[19,9], A. Zimmermann[83], G. Zinovjev[2], Y. Zoccarato[109], M. Zynovyev[2]

[1] Benemérita Universidad Autónoma de Puebla, Puebla, Mexico
[2] Bogolyubov Institute for Theoretical Physics, Kiev, Ukraine
[3] Budker Institute for Nuclear Physics, Novosibirsk, Russia
[4] California Polytechnic State University, San Luis Obispo, California, United States
[5] Centre de Calcul de l'IN2P3, Villeurbanne, France
[6] Centro de Aplicaciones Tecnológicas y Desarrollo Nuclear (CEADEN), Havana, Cuba
[7] Centro de Investigaciones Energéticas Medioambientales y Tecnológicas (CIEMAT), Madrid, Spain
[8] Centro de Investigación y de Estudios Avanzados (CINVESTAV), Mexico City and Mérida, Mexico
[9] Centro Fermi – Centro Studi e Ricerche e Museo Storico della Fisica "Enrico Fermi", Rome, Italy
[10] Chicago State University, Chicago, United States
[11] China Institute of Atomic Energy, Beijing, China
[12] Commissariat à l'Energie Atomique, IRFU, Saclay, France
[13] Departamento de Física de Partículas and IGFAE, Universidad de Santiago de Compostela, Santiago de Compostela, Spain
[14] Department of Physics Aligarh Muslim University, Aligarh, India
[15] Department of Physics and Technology, University of Bergen, Bergen, Norway
[16] Department of Physics, Ohio State University, Columbus, Ohio, United States
[17] Department of Physics, Sejong University, Seoul, South Korea
[18] Department of Physics, University of Oslo, Oslo, Norway
[19] Dipartimento di Fisica dell'Università and Sezione INFN, Bologna, Italy
[20] Dipartimento di Fisica dell'Università and Sezione INFN, Trieste, Italy
[21] Dipartimento di Fisica dell'Università and Sezione INFN, Cagliari, Italy
[22] Dipartimento di Fisica dell'Università and Sezione INFN, Padova, Italy

JHEP01(2012)128

[23] Dipartimento di Fisica dell'Università 'La Sapienza' and Sezione INFN, Rome, Italy
[24] Dipartimento di Fisica e Astronomia dell'Università and Sezione INFN, Catania, Italy
[25] Dipartimento di Fisica 'E.R. Caianiello' dell'Università and Gruppo Collegato INFN, Salerno, Italy
[26] Dipartimento di Fisica Sperimentale dell'Università and Sezione INFN, Turin, Italy
[27] Dipartimento di Scienze e Tecnologie Avanzate dell'Università del Piemonte Orientale and Gruppo Collegato INFN, Alessandria, Italy
[28] Dipartimento Interateneo di Fisica 'M. Merlin' and Sezione INFN, Bari, Italy
[29] Division of Experimental High Energy Physics, University of Lund, Lund, Sweden
[30] European Organization for Nuclear Research (CERN), Geneva, Switzerland
[31] Fachhochschule Köln, Köln, Germany
[32] Faculty of Engineering, Bergen University College, Bergen, Norway
[33] Faculty of Mathematics, Physics and Informatics, Comenius University, Bratislava, Slovakia
[34] Faculty of Nuclear Sciences and Physical Engineering, Czech Technical University in Prague, Prague, Czech Republic
[35] Faculty of Science, P.J. Šafárik University, Košice, Slovakia
[36] Frankfurt Institute for Advanced Studies, Johann Wolfgang Goethe-Universität Frankfurt, Frankfurt, Germany
[37] Gangneung-Wonju National University, Gangneung, South Korea
[38] Helsinki Institute of Physics (HIP) and University of Jyväskylä, Jyväskylä, Finland
[39] Hiroshima University, Hiroshima, Japan
[40] Hua-Zhong Normal University, Wuhan, China
[41] Indian Institute of Technology, Mumbai, India
[42] Institut de Physique Nucléaire d'Orsay (IPNO), Université Paris-Sud, CNRS-IN2P3, Orsay, France
[43] Institute for High Energy Physics, Protvino, Russia
[44] Institute for Nuclear Research, Academy of Sciences, Moscow, Russia
[45] Nikhef, National Institute for Subatomic Physics and Institute for Subatomic Physics of Utrecht University, Utrecht, Netherlands
[46] Institute for Theoretical and Experimental Physics, Moscow, Russia
[47] Institute of Experimental Physics, Slovak Academy of Sciences, Košice, Slovakia
[48] Institute of Physics, Bhubaneswar, India
[49] Institute of Physics, Academy of Sciences of the Czech Republic, Prague, Czech Republic
[50] Institute of Space Sciences (ISS), Bucharest, Romania
[51] Institut für Informatik, Johann Wolfgang Goethe-Universität Frankfurt, Frankfurt, Germany
[52] Institut für Kernphysik, Johann Wolfgang Goethe-Universität Frankfurt, Frankfurt, Germany
[53] Institut für Kernphysik, Technische Universität Darmstadt, Darmstadt, Germany
[54] Institut für Kernphysik, Westfälische Wilhelms-Universität Münster, Münster, Germany
[55] Instituto de Ciencias Nucleares, Universidad Nacional Autónoma de México, Mexico City, Mexico
[56] Instituto de Física, Universidad Nacional Autónoma de México, Mexico City, Mexico
[57] Institut of Theoretical Physics, University of Wroclaw
[58] Institut Pluridisciplinaire Hubert Curien (IPHC), Université de Strasbourg, CNRS-IN2P3, Strasbourg, France
[59] Joint Institute for Nuclear Research (JINR), Dubna, Russia

JHEP01(2012)128

[60] KFKI Research Institute for Particle and Nuclear Physics, Hungarian Academy of Sciences, Budapest, Hungary
[61] Kharkiv Institute of Physics and Technology (KIPT), National Academy of Sciences of Ukraine (NASU), Kharkov, Ukraine
[62] Kirchhoff-Institut für Physik, Ruprecht-Karls-Universität Heidelberg, Heidelberg, Germany
[63] Korea Institute of Science and Technology Information
[64] Laboratoire de Physique Corpusculaire (LPC), Clermont Université, Université Blaise Pascal, CNRS–IN2P3, Clermont-Ferrand, France
[65] Laboratoire de Physique Subatomique et de Cosmologie (LPSC), Université Joseph Fourier, CNRS-IN2P3, Institut Polytechnique de Grenoble, Grenoble, France
[66] Laboratori Nazionali di Frascati, INFN, Frascati, Italy
[67] Laboratori Nazionali di Legnaro, INFN, Legnaro, Italy
[68] Lawrence Berkeley National Laboratory, Berkeley, California, United States
[69] Lawrence Livermore National Laboratory, Livermore, California, United States
[70] Moscow Engineering Physics Institute, Moscow, Russia
[71] National Institute for Physics and Nuclear Engineering, Bucharest, Romania
[72] Niels Bohr Institute, University of Copenhagen, Copenhagen, Denmark
[73] Nikhef, National Institute for Subatomic Physics, Amsterdam, Netherlands
[74] Nuclear Physics Institute, Academy of Sciences of the Czech Republic, Řež u Prahy, Czech Republic
[75] Oak Ridge National Laboratory, Oak Ridge, Tennessee, United States
[76] Petersburg Nuclear Physics Institute, Gatchina, Russia
[77] Physics Department, Creighton University, Omaha, Nebraska, United States
[78] Physics Department, Panjab University, Chandigarh, India
[79] Physics Department, University of Athens, Athens, Greece
[80] Physics Department, University of Cape Town, iThemba LABS, Cape Town, South Africa
[81] Physics Department, University of Jammu, Jammu, India
[82] Physics Department, University of Rajasthan, Jaipur, India
[83] Physikalisches Institut, Ruprecht-Karls-Universität Heidelberg, Heidelberg, Germany
[84] Purdue University, West Lafayette, Indiana, United States
[85] Pusan National University, Pusan, South Korea
[86] Research Division and ExtreMe Matter Institute EMMI, GSI Helmholtzzentrum für Schwerionenforschung, Darmstadt, Germany
[87] Rudjer Bošković Institute, Zagreb, Croatia
[88] Russian Federal Nuclear Center (VNIIEF), Sarov, Russia
[89] Russian Research Centre Kurchatov Institute, Moscow, Russia
[90] Saha Institute of Nuclear Physics, Kolkata, India
[91] School of Physics and Astronomy, University of Birmingham, Birmingham, United Kingdom
[92] Sección Física, Departamento de Ciencias, Pontificia Universidad Católica del Perú, Lima, Peru
[93] Sezione INFN, Cagliari, Italy
[94] Sezione INFN, Bari, Italy
[95] Sezione INFN, Turin, Italy
[96] Sezione INFN, Bologna, Italy
[97] Sezione INFN, Catania, Italy

JHEP01(2012)128

[98] Sezione INFN, Trieste, Italy
[99] Sezione INFN, Rome, Italy
[100] Sezione INFN, Padova, Italy
[101] Soltan Institute for Nuclear Studies, Warsaw, Poland
[102] SUBATECH, Ecole des Mines de Nantes, Université de Nantes, CNRS-IN2P3, Nantes, France
[103] Technical University of Split FESB, Split, Croatia
[104] The Henryk Niewodniczanski Institute of Nuclear Physics, Polish Academy of Sciences, Cracow, Poland
[105] The University of Texas at Austin, Physics Department, Austin, TX, United States
[106] Universidad Autónoma de Sinaloa, Culiacán, Mexico
[107] Universidade de São Paulo (USP), São Paulo, Brazil
[108] Universidade Estadual de Campinas (UNICAMP), Campinas, Brazil
[109] Université de Lyon, Université Lyon 1, CNRS/IN2P3, IPN-Lyon, Villeurbanne, France
[110] University of Houston, Houston, Texas, United States
[111] University of Technology and Austrian Academy of Sciences, Vienna, Austria
[112] University of Tennessee, Knoxville, Tennessee, United States
[113] University of Tokyo, Tokyo, Japan
[114] University of Tsukuba, Tsukuba, Japan
[115] Eberhard Karls Universität Tübingen, Tübingen, Germany
[116] Variable Energy Cyclotron Centre, Kolkata, India
[117] V. Fock Institute for Physics, St. Petersburg State University, St. Petersburg, Russia
[118] Warsaw University of Technology, Warsaw, Poland
[119] Wayne State University, Detroit, Michigan, United States
[120] Yale University, New Haven, Connecticut, United States
[121] Yerevan Physics Institute, Yerevan, Armenia
[122] Yildiz Technical University, Istanbul, Turkey
[123] Yonsei University, Seoul, South Korea
[124] Zentrum für Technologietransfer und Telekommunikation (ZTT), Fachhochschule Worms, Worms, Germany

[i] Deceased
[ii] Also at: Dipartimento di Fisica dell'Universita, Udine, Italy
[iii] Also at: M.V.Lomonosov Moscow State University, D.V.Skobeltsyn Institute of Nuclear Physics, Moscow, Russia
[iv] Also at: "Vinča" Institute of Nuclear Sciences, Belgrade, Serbia

JHEP01(2012)128